

Original Article

Cite this article: Moazzen M, Salimi Z, Rolland Y, Bröcker M, and Hajjalioghli R (2020) Protolith nature and P – T evolution of Variscan metamorphic rocks from the Allahyarlu complex, NW Iran. *Geological Magazine* **157**: 1853–1876. <https://doi.org/10.1017/S0016756820000102>

Received: 29 May 2019

Revised: 18 January 2020

Accepted: 29 January 2020

First published online: 18 March 2020

Keywords:


metapelite; amphibolite; P – T estimates; active continental margin; Variscan orogeny; NW Iran

Author for correspondence:

Mohssen Moazzen,

Email: mohssen.moazzen@ucentralasia.org

Protolith nature and P – T evolution of Variscan metamorphic rocks from the Allahyarlu complex, NW Iran

Mohssen Moazzen^{1,2} , Zohreh Salimi², Yann Rolland³, Michael Bröcker⁴ and Robab Hajjalioghli²

¹School of Arts and Sciences, University of Central Asia, Khorog, 736000, Tajikistan; ²Department of Earth Sciences, University of Tabriz, 51666, Tabriz, Iran; ³Université Côte d'Azur, CNRS, OCA, IRD, Géoazur, Sophia Antipolis, France and ⁴Institut für Mineralogie, Westfälische-Wilhelms Universität Münster, Münster, Germany

Abstract

Metamorphic rocks associated with ophiolitic rocks occur on the eroded surface of a NW–SE-trending anticline in the Allahyarlu area, NW Iran, between the Caucasus and Zagros orogenic belts. Metapelitic rocks consist mainly of quartz, muscovite chlorite, altered biotite and garnet. S_1 is the pervasive schistosity, wrapping garnet, which is folded by the second schistosity (S_2). The amphibolite records only one phase of deformation as the main lineation. The rocks experienced metamorphism up to the amphibolite facies, then overprinted by greenschist facies condition. Thermobarometry indicates an average pressure of *c.* 5 kbar and an average temperature of *c.* 600 °C for the amphibolite facies metamorphism, corresponding to a ~ 33 °C km⁻¹ geothermal gradient in response to a thick magmatic arc setting. Greenschist facies metamorphism shows re-equilibration of the rocks during exhumation. Amphibolites whole rock geochemistry shows trace elements patterns similar to both island arc and back-arc basin basalts, suggesting that the protolith-forming magma of the amphibolites was enriched at shallow to medium depth of a subduction system. Negative Nb anomaly and slight enrichment in light rare earth elements (LREE) and large-ion lithophile elements (LILE) of the amphibolites indicate arc-related magmatism for their protolith and a back-arc sialic setting for their formation. ⁴⁰Ar–³⁹Ar dating on muscovite separated from two gneiss samples, and hornblende separated from three amphibolite samples, documents a Variscan (326–334 Ma) age. The magmatic and metamorphic rock association of the Allahyarlu area suggests the existence of an active continental margin arc during the Variscan orogeny, without clear evidence for a continental collision.

1. Introduction

Palaeotethys-related ophiolites and metamorphic rocks mark the northward subduction of the ocean crust and subsequent collision of Gondwana and Laurasia (Stampfli & Borel, 2002; Rossetti *et al.* 2017). Carboniferous metamorphic rocks (Variscan) are important in this regard, and are ascribed to high-pressure metamorphism during subduction of the oceanic crust (Faryad & Kachlik, 2013; Omrani *et al.* 2013; Rossetti *et al.* 2017) or high-temperature metamorphism by crustal thickening and subsequent thinning by erosion (Gerdes *et al.* 2000) or magma underplating (Büttner & Kruhl, 1997). The Variscan orogeny is related to the collision of Gondwanan terrains with Laurasia during the Late Palaeozoic (mainly 300–350 Ma; Kröner & Romer, 2013). Variscan magmatic and metamorphic rocks are exposed in the central and eastern basement rocks of the Pontides (to the west of the study area; Okay & Şahintürk, 1997; Topuz *et al.* 2004a, b; 2007; Dokuz, 2011; Dokuz *et al.* 2011; Ustaömer *et al.* 2013), in the Caucasus (to the north of the study area; Somin, 1991; Perchuk & Philippot, 1997), the Transcaucasus (Zakariadze *et al.* 1998; Gamkrelidze *et al.* 2011; Mayringer *et al.* 2011) and in Central Iran (Bagheri & Stampfli, 2008; Kargaranbafghi *et al.* 2015; Zanchi *et al.* 2015).

There are several models for the formation of the Variscan metamorphic and igneous rocks in the Pontides, Transcaucasus and Balkan regions (Ustaömer *et al.* 2013). These rocks are formed along the southern margin of Eurasia, due to rifting at the northern margin of Gondwana and drifting of the continental slivers and their accretion to the south Eurasia margin in the Carboniferous (Adamia *et al.* 1977; Dercourt *et al.* 1993; Stampfli & Borel, 2002; Nikishin *et al.* 2011). Ustaömer & Robertson (1993) considered the closure of a marginal back-arc basin in response to the pre-Late Jurassic southward subduction and accretion. Some researchers assumed either a southward subduction for the Palaeotethys (Şengör & Yilmaz, 1981; Şengör *et al.* 1984; Göncüoğlu *et al.* 2000; Romano *et al.* 2006; Zulauf *et al.* 2007) or a combined northward and southward subduction of the Rheic Ocean (Dokuz *et al.* 2011). Alternative models propose that northward subduction below Eurasia accreted several Gondwana-derived

continental blocks during Carboniferous–Permian times to the southern margin of Eurasia. This caused the closure of the Rheic Ocean and the generation of a Cordilleran-type orogeny (Nikishin *et al.* 2011). Rolland *et al.* (2011) explained the Variscan high-temperature metamorphism and related magmatism as due to an active margin setting which followed the accretion of these Gondwana-derived blocks to Eurasia. In this model, metamorphism could have been achieved without any collisional thickening. Due to scarcity of studies on the Palaeotethys-related rocks in Iran, it is difficult to assess the timing and geodynamics of continental assembly during the Palaeozoic. A relatively small tectonic window of metamorphic rocks, composed of pelitic, psammitic and mafic protolith compositions along with serpentized harzburgite, gabbro and diabase, occurs on the eroded surface of a NW–SE-trending anticline in the Allahyarlu area, NW Iran, known as the Allahyarlu complex (Babakhani & Nazer, 1991; Fig. 1). These rocks are unconformably covered by Late Cretaceous carbonate and volcanic units. The complex is located at a crucial position regarding the exact location of the Palaeotethys and Neotethys sutures in NW Iran, the Caucasus and eastern Turkey (Fig. 1a). Some researchers consider the Allahyarlu complex as an ophiolitic mélangé (e.g. Babakhani & Nazer, 1991; Barzegar & Pourkermani, 2011; M. Sudi Ajirlu, unpub. MSc thesis, Univ. Tabriz, 2011). They interpret these rocks as the southern continuation of the Sevan–Akeru ophiolite belt of the lesser Caucasus (Stöcklin, 1977; Stampfli, 1978; Berberian & King, 1981; Boulin, 1988; Galoyan *et al.* 2009), while Eftekharijad *et al.* (1993) argued that the Allahyarlu complex is a continuation of the south Mashhad ophiolites (Shafaii Moghadam *et al.* 2015) and/or the Shanderman and Masuleh complexes (Omran *et al.* 2013; Rossetti *et al.* 2017) along the Palaeotethys suture in North Iran (Fig. 1a). However, to fulfil the Penrose ophiolite definition, the Allahyarlu complex lacks some typical components such as pillow basalts and sheeted dykes, and serpentized peridotites only have limited exposure. The metamorphic rocks are thrust on the ophiolite mélangé. There is no published account on the petrology, geochemistry and geochronology of the Allahyarlu rock suite. Babakhani & Nazer (1991) considered the Early Cimmerian orogenic phase responsible for metamorphism in the area. On the other hand, Stampfli & Borel (2002) interpreted this type of rock as part of a Cimmerian ribbon, which rifted from Gondwana during the Late Permian and collided with Eurasia during the Late Triassic. This event is thought to terminate the history of Palaeotethys subduction and resulted in the accretion or obduction of NW Iran Neotethys ophiolites. Besides, ongoing intra-oceanic subduction to the north of the Anatolian–Armenian blocks in Jurassic time shows that there was no Cimmerian continental fragment along the Izmir–Ankara–Erzincan suture (Rolland *et al.* 2012; Topuz *et al.* 2013; Hässig *et al.* 2015). Therefore, the question of the correspondence of the Sevan–Akeru suture in NW Iran is raised: is it the continuation of the Allahyarlu suture or should it rather be considered as the lateral continuation of the Zagros suture (through the Khoy ophiolite; Khalatbari Jafari & Babaie, 2016; Shafaii Moghadam *et al.* 2018), offset by a N–S transform fault (e.g. Rolland, 2017)? Further, the age of metamorphism of the Allahyarlu complex is put into question, as there is no absolute geochronological constraint on these rocks. Babakhani & Nazer (1991) attributed folding of the Cretaceous sediments and following magmatism of the area to the impact of a Laramide-type (active margin) orogeny, corresponding to ongoing subduction below southern Iran. Barzegar & Pourkermani (2011) consider folding of Palaeocene

to Eocene sandstones and conglomerates in the area as a result of the Late Alpine orogeny. However, Allahyarlu-complex metamorphism may rather correspond to an older tectonic event like the Variscan high-pressure (HP) metamorphism evidenced by Rossetti *et al.* (2017) to the west of the Caspian Sea along the same Allahyarlu–Hovai fault. The relationship of the Allahyarlu-complex metamorphism to Neotethys subductions, Alpine collisions or a preserved older tectonic phase is not yet resolved. In this paper, we consider the metamorphic rocks, which form the crystalline basement representing the oldest units in the Allahyarlu area. Field relationships and petrography as well as whole rock and mineral chemistry of these rocks are reported and complemented by $^{40}\text{Ar}/^{40}\text{Ar}$ dating on white mica and amphibole in meta-psammitic and metabasic lithologies, respectively. We will show that the oldest rocks of the Allahyarlu complex were metamorphosed up to the amphibolite facies during the Hercynian orogeny and thus are unrelated to the Cimmerian phase. This result is used to discuss the geodynamic context of NW Iran in relation to adjacent areas in east Anatolia–Armenia and the Lesser Caucasus.

2. Geological setting of the Allahyarlu area

Northwest Iran, east Anatolia and the Lesser Caucasus constitute a complicated geological terrain. There are many studies and opinions on the geology of this area, but there is no general consensus on its geodynamic evolution. NW Iran is attributed to different geological and tectonic subdivisions. It is located in the west Alborz–Azerbaijan (Nabavi, 1976), Alborz range (Stöcklin, 1968), Western Alborz (Stampfli, 1978) and Central Iran (Aghanabati, 2004) geological units. The Alborz range is a composite poly-orogenic belt within the Alpine–Himalayan orogen, the main geomorphological features of which are brought about by Alpine orogeny. The Allahyarlu area in Iranian Azerbaijan is located between the Caucasus and Zagros orogenic belts, at the northern boundary of the Ahar Block (Fig. 1b; Stöcklin, 1968; Berberian & King, 1981; Sudi Ajirlu & Moazzen, 2014). The late Alpine orogenic phase is evidenced by folding of Eocene to Oligocene/Miocene flysch-type sediments. The Ahar Block basement is characterized by greenschist- to amphibolite-facies psammities, metapelites and metabasites, which are the subject of this study. The study area can be divided into three geologic units: (i) old metamorphic rocks, (ii) ophiolite mélangé and Cretaceous sedimentary rocks and (iii) Tertiary volcanic rocks. The basement rocks and overlying Cretaceous sediments have been thrust onto the Pre- to Late Cretaceous ophiolite rock suite, comprising ultramafic, mafic and intermediate igneous rocks (Fig. 2). All these rock units are subsequently folded into a relatively small (~12 km long and 2 km across) anticline; and later a further low-angle fault has cut out the core of the anticline. The older rocks are covered by Late Cretaceous sedimentary and volcanic units, and thick outcrops of Palaeocene–Eocene volcanic and pyroclastic rocks (Fig. 2). Metamorphic rocks are exposed on an eroded surface in the core of the anticline (Fig. 3a). The main faults cross-cutting the basement are top-to-the-south thrusts along the anticline axis, which have juxtaposed the basement units onto the younger rocks. Some minor NE–SW and NW–SE-trending strike-slip faults also cross-cut most units. The metamorphic and ophiolitic rocks are exposed only at the anticline core and are covered by widespread Palaeogene volcanic rocks in other parts of the area. The contacts between the ophiolitic rocks and the metamorphic rocks are defined by

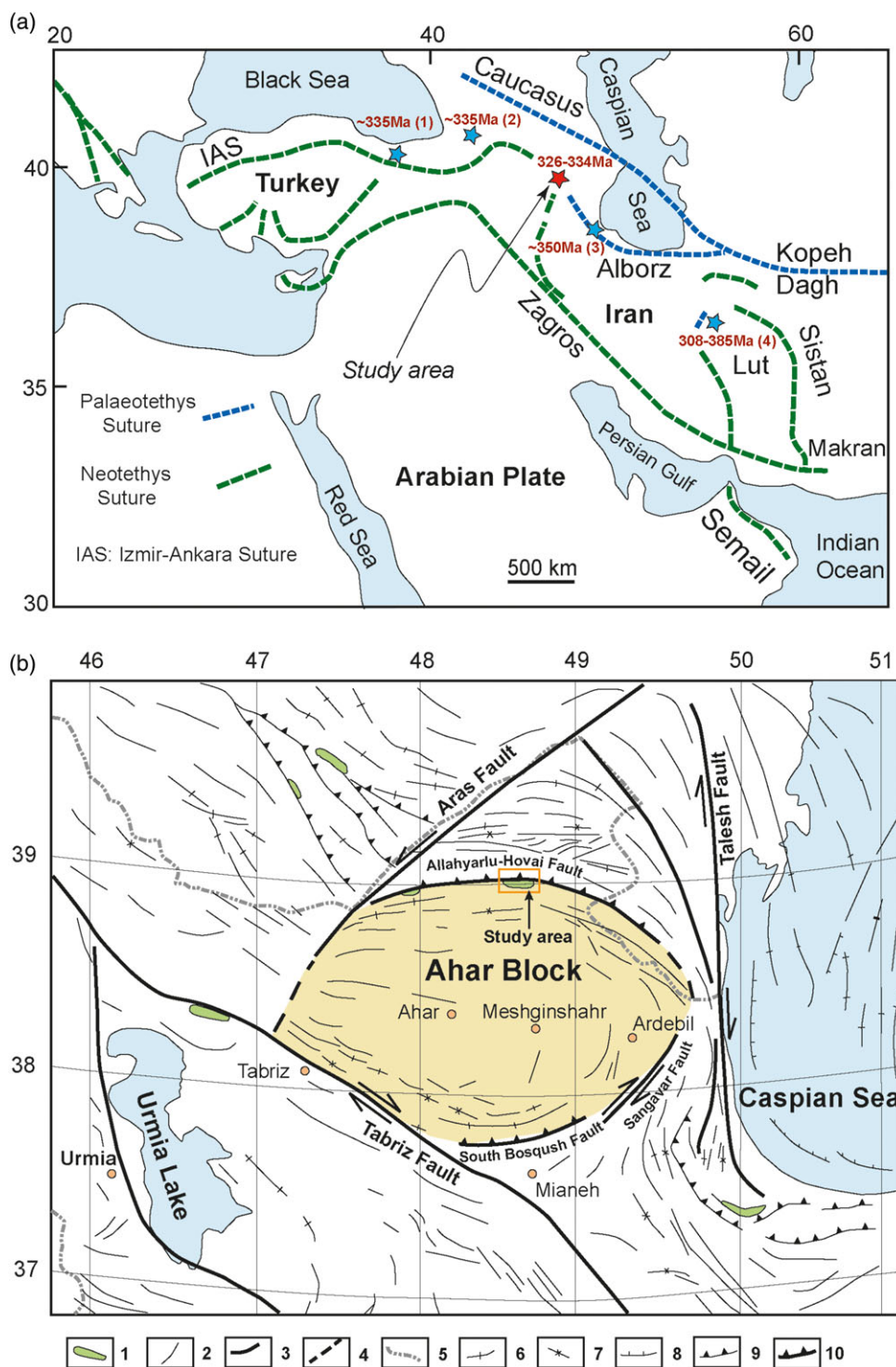


Fig. 1. (Colour online) (a) The locality of the study area in NW Iran and in relation to the main Neotethys and Palaeotethys sutures in the Middle East. Some examples of Variscan metamorphic rocks are shown with peak metamorphic ages: (1) Eastern Pontides (Topuz *et al.* 2007); (2) Armenia (Rolland *et al.* 2011); (3) Rasht (Rossetti *et al.* 2017); (4) Anarak (Buchs *et al.* 2013). (b) The study area in the northern part of the Ahhar Block. The legends are: 1. remnants of the oceanic crust; 2. local structural trends; 3. main faults; 4. hidden faults; 5. country borders; 6. anticline; 7. syncline; 8. depression; 9. thrust; 10. Allahyarlu–Hovai thrust.

faults. The Pre- to Late Cretaceous ophiolite mélangé is composed of serpentinized peridotite, gabbro, diabase and pelagic limestone with minor amounts of radiolarian chert. Serpentinized peridotites are mainly restricted to the shear zones and appear as sporadic lenses or blocks. The protolith was harzburgite in which spinel chemistry is in favour of a supra-subduction zone and fore-arc

setting (Z. Salimi, unpub. PhD thesis, Univ. Tabriz, 2019). Gabbros in the ophiolitic mélangé are isotropic, and associated with small outcrops of diorite and micro-diorite. Diabase appears mainly as dykes. The Late Cretaceous units are formed by a sequence of deep marine fossil-bearing limestone of Lower Cenomanian age (Babakhani & Nazer, 1991), a layer of andesite

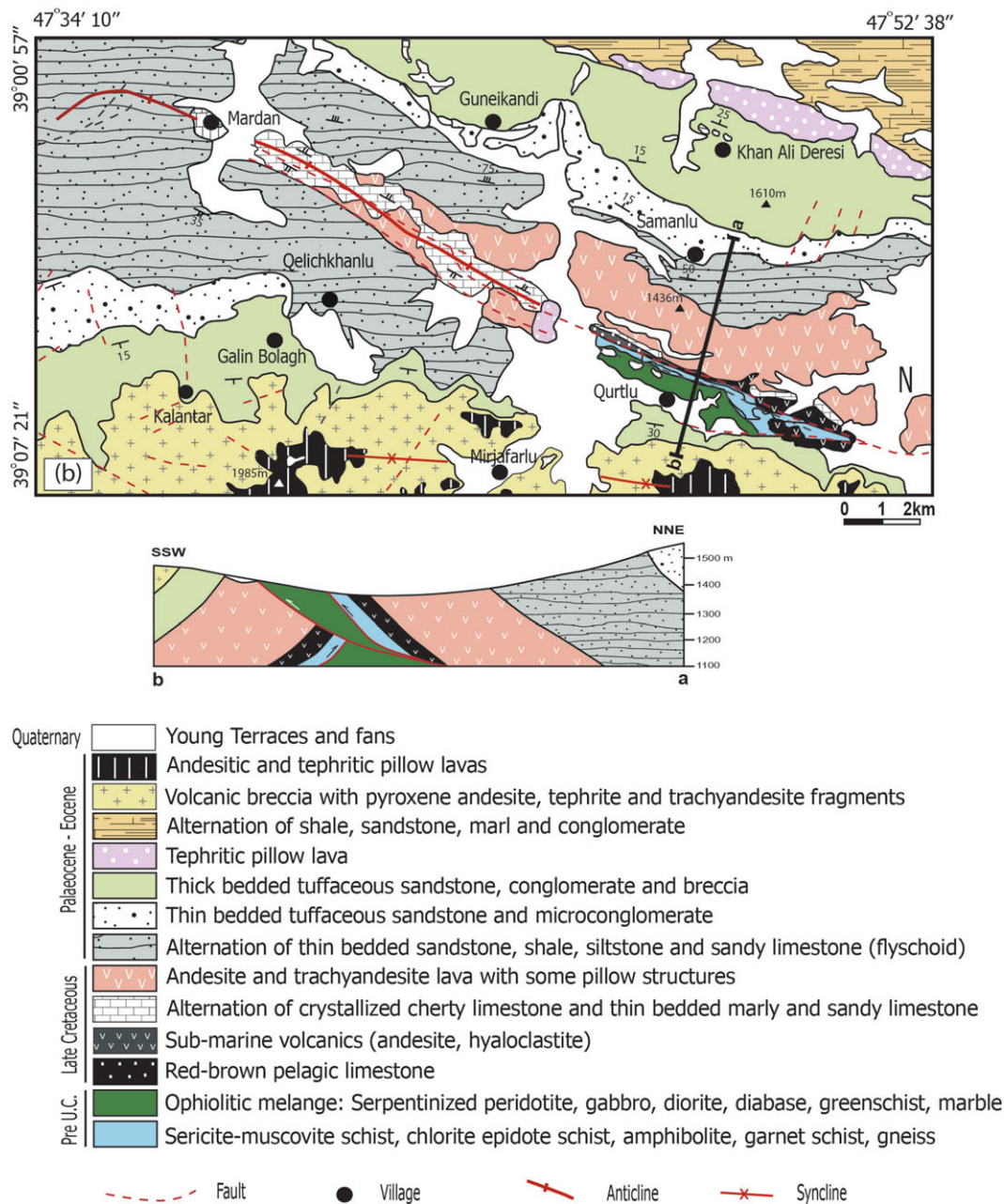


Fig. 2. (Colour online) The geological map and cross-section of the studied area, modified from Babakhani & Nazer (1991).

and hyaloclastite, sandy limestone with thin chert layers and spilitic andesite with some pillow structures. These rocks are thrust onto Campanian and Maastrichtian sediments (Babakhani & Nazer, 1991). Metamorphosed mafic rocks are scarce and are mainly represented by amphibolites (Fig. 3b) with alternating dark hornblende-rich and pale plagioclase-rich layers, with a distinct lineation. The main metamorphic rocks of the area are garnet ± chlorite white mica schists, which have a pelitic to semi-pelitic protolith composition. The pelitic and semi-pelitic rocks show a well-developed high-temperature mineral foliation (Fig. 3c), underlined by garnet + white mica with a main NW–SE direction, parallel to the anticline axis. Some slightly metamorphosed (greenschist facies) mafic dykes occasionally cross-cut the metapelitic schists. Garnet gneisses are present as massive bodies with a folded foliation defined by mica- and quartz-rich layers

(Fig. 3d). Garnet-free gneisses occur as interlayers in pelitic schists, possibly indicating a shallow turbiditic environment of deposition for the parental rocks. In some parts of the gneisses, the quartz-rich layers reach a thickness of up to 30 cm and form distinct quartzite layers.

3. Analytical methods

Whole rock analyses were carried out on 14 representative samples (8 amphibolites, 4 metapelitic schists, 2 gneisses) that were selected from a rock suite of more than 150 samples. Whole rock analyses were performed using X-ray fluorescence (XRF) and inductively coupled plasma mass spectrometer (ICP-MS) methods at the Institut des Géosciences de l'Environnement, Université Grenoble Alpes, France, and at Actlabs laboratories in Ontario,

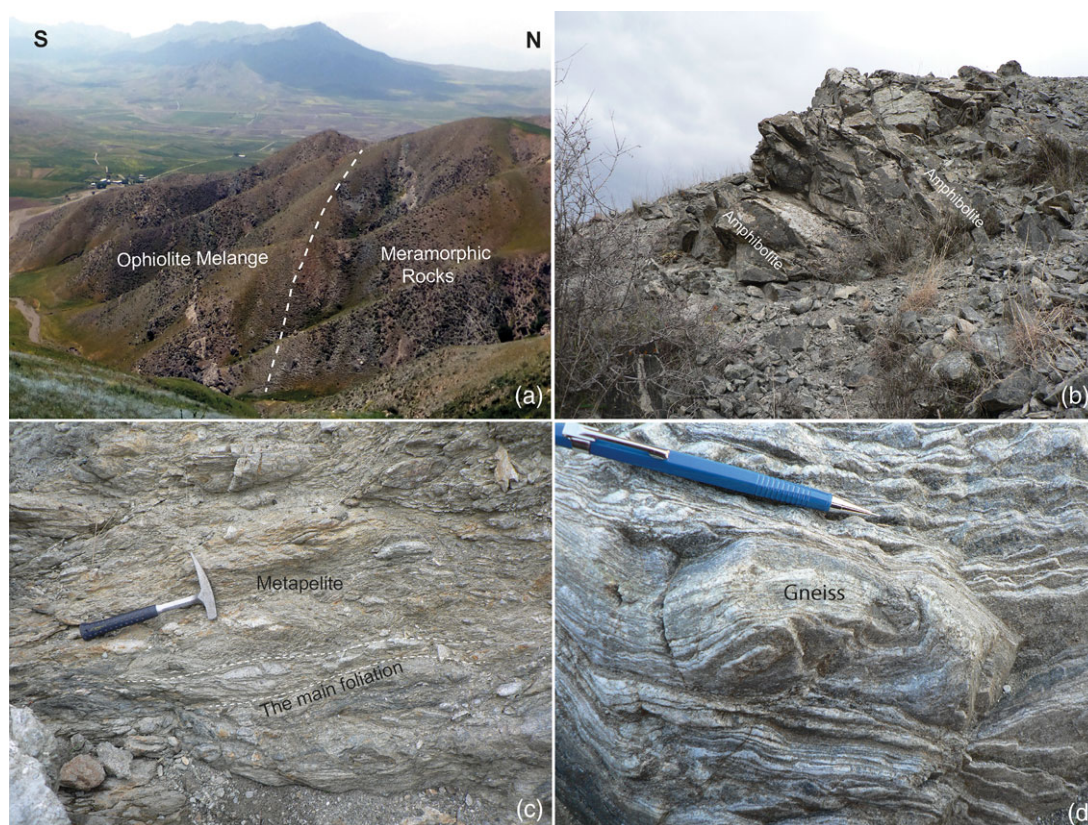


Fig. 3. (Colour online) (a) Outcrop of ophiolitic and metamorphic rocks at the erosion surface on the Allahyarlu anticline. (b) Outcrop of amphibolites. (c) Metapelitic rocks with pervasive S_1 foliation. (d) Outcrop of gneiss with quartz- and plagioclase-rich pale and biotite-rich dark bands.

Canada (4Litho-Research analytical package). About 1 kg of each sample was crushed using a steel-jaw mill and was pulverized to 200 mesh. A known amount of sample was mixed with lithium metaborate and fused on a gas heater. The resulting glass discs were used for XRF analyses of major oxides. After digestion in acid and dilution they were used for minor and trace elements analyses using an ICP-MS. International standards were used for calibrations. The uncertainties for the major oxides are better than 2 % and for the minor and trace elements better than 5 %. Mineral chemical analyses were done using a Japan Electron Optics Ltd (JEOL) JXA-8530 F Superprobe at the Institut für Mineralogie, Universität Münster, Germany. The acceleration voltage during analyses was 15 kv, with 15 nA specimen current and counting times of 10 s for the peak and 5 s for the background (except for Na and K for which 5 s peak and 2.5 s background counting time was applied). Natural and synthetic standards were used for calibration. The raw data were processed by the ZAF software. The quality of electron-probe microanalysis (EPMA) data were checked regarding the total oxides analysed and the formula unit calculated for the minerals. $^{40}\text{Ar}/^{39}\text{Ar}$ dating on muscovite and hornblende separates from the metamorphic rocks was performed at UMR Géosciences Azur, Nice, France. The samples were crushed to a 500–800 μm size fraction and cleaned in an ultrasonic bath. Muscovite grains were carefully hand-picked under a binocular microscope to select only grains without evidence of alteration or inclusions. These grains were packaged in aluminium foil and irradiated along with hornblende neutron fluence monitor Hb3gr, with an age of 1072 Ma (Turner *et al.* 1971), in the McMaster University nuclear reactor, Hamilton, Canada. Argon isotopic interferences on K and Ca were determined by irradiation

of KF and CaF_2 pure salts from which the following correction factors were obtained: $(^{36}\text{Ar}/^{37}\text{Ar})\text{Ca} = 0.000288 \pm 0.000016$; $(^{39}\text{Ar}/^{37}\text{Ar})\text{Ca} = 0.000727 \pm 0.000041$; $(^{40}\text{Ar}/^{39}\text{Ar})\text{k} = 0.00969 \pm 0.00038$; $(^{38}\text{Ar}/^{39}\text{Ar})\text{k} = 0.01297 \pm 0.00045$. All samples were analysed with a device consisting of: (a) an IR- CO_2 laser of 100 kHz used at 5–15 % during 60 s, (b) a lens system for beam focusing, (c) a steel chamber, maintained at 10^{-8} – 10^{-9} bar, with a drilled copper plate, (d) an inlet line for purification of gases including two Zr–Al getters and (e) a multi-collector mass spectrometer (Argus VI from Thermo-Fisher). The ARGUS VI spectrometer has a mass resolution of 225–250 and a measured sensitivity of 7×10^{-14} mol V^{-1} at 200 μA trap current. The high-mass Faraday detector is fitted with a 1011 Ω resistor and is used specifically for measuring the $^{40}\text{Ar}^+$ beam intensity. The Faraday detectors used for other Ar isotope measurements are fitted with 1012 Ω resistors. Direct measurement of collector noise for ten separate runs gave averages of 4×10^6 V on the 1011 Ω circuit and 1×10^5 V on the 1012 Ω circuit. Collector gain calibration is performed by the computer-controlled application of predetermined voltages to each collector. Over the course of 1 year, the relative gain between collectors did not exceed 19 ppm. The compact discrete dynode electron multiplier channel was used for single collector peak jumping measurements. System blanks were measured every three experiments. The blanks typically accounted for less than 0.06 % of the ^{40}Ar , 0.6–3.81 % of the ^{38}Ar , and 0.12–0.71 % of the ^{36}Ar . Mass discrimination for the mass spectrometer was monitored by regularly analysing air pipette volumes. We used ArArCalc © software v2.5.2 for data processing (Koppers, 2002). Decay constants are those given by Steiger & Jäger (1977). Uncertainties on apparent and plateau ages are given at the

Table 1. Mineral assemblages (mineral name abbreviations after Whitney & Evans, 2010)

Mica schist and gneiss												
Sample	GPS/GR	Qtz	Chl	Grt	Bt	Ms	Opq	Zrn	Tur	Ttn	Ab	
ZS-13*,▲	N38° 53' 23.3" E47° 47' 46.2"	++	+	++	+	++	+	o	o	–	–	
ZS-42*	N38° 53' 42.2" E47° 47' 32.3"	++	+	++	+	++	+	o	o	–	o	
ZS-28*	N38° 53' 23.2" E47° 47' 29.8"	++	–	++	+	++	–	–	–	–	o	
ZS-2N*	N38° 53' 55.7" E47° 46' 31.9"	++	–	++	–	++	+	–	o	–	o	
ZS-18-19*	N38° 53' 57.2" E47° 46' 27.7"	++	–	++	+	++	–	–	–	–	–	
ZS-1-12*,◆	N38° 53' 21.0" E47° 47' 26.2"	++	–	++	+	++	–	–	o	–	o	
ZS-1-15*,◆	N38° 53' 32.7" E37° 46' 51.8"	++	–	++	+	++	–	–	o	o	–	
Amphibolites												
Sample	GPS/GR	Pl	Hbl	Ep	Grt	Bt	Ttn	Cal	Zrn	Opq	Qrt	Act-Tr
ZS-3B*,◆	38° 53' 14.9" 47° 48' 32.7"	++	++	++	–	–	+	o	–	o	+	–
ZS-43*,◆	38° 53' 27.6" 47° 47' 42.0"	++	++	–	–	–	+	–	o	o	–	–
ZS-1-14*	38° 53' 32.1" 47° 47' 3.9"	++	++	–	++	+	+	–	o	o	o	–
AZ-18-14	38° 53' 30.2" 47° 47' 4.2"	++	++		++							
AZ-18-11	38° 53' 30.3" 47° 47' 4.1"	++	++	++								
AZ-18-9	38° 53' 31.4" 47° 47' 4.0"	++	++		++							
AZ-18-18	38° 53' 31.0" 47° 47' 3.8"	++	++		++							
AZ-18-13	38° 53' 31.3" 47° 47' 3.9"	++	++		++							
AZ-18-19	38° 53' 31.3" 47° 47' 3.8"	++	++									

++ Major phase; + minor phase; o accessory phase. * EPMA. ▲ Whole-rock analysis. ◆ ⁴⁰Ar/³⁹Ar dating.

1σ level including the uncertainty on the ⁴⁰Ar*/³⁹Ar ratio of the monitor. The one-sigma errors reported on plateau, isochron and total gas ages include the error on the irradiation factor *J*. Atmospheric ⁴⁰Ar was estimated using a value of the initial ⁴⁰Ar/³⁶Ar of 295.5.

4. Rock descriptions and mineral compositions

The pelitic schists of the study area include garnet–chlorite–muscovite and garnet–biotite–muscovite schists (Table 1). The major minerals in the chlorite-bearing schists are quartz, chlorite,

muscovite and garnet, the minor phases are plagioclase and Fe-oxides and accessory phases are graphite and tourmaline. Foliation is well developed in these rocks, and a crenulation cleavage can be observed (Fig. 4a; mineral name abbreviations are from Whitney & Evans, 2010). The main textures are lepidoblastic and porphyroblastic. Garnet occurs as idioblastic porphyroblasts, up to 1.5 mm across, with inclusions of quartz and muscovite. About 1 mm long plagioclase crystals are occasionally present as porphyroblasts. Fine- (0.5 mm) to relatively coarse (1.5 mm)-grained biotite in the biotite–garnet–muscovite schist is extensively altered

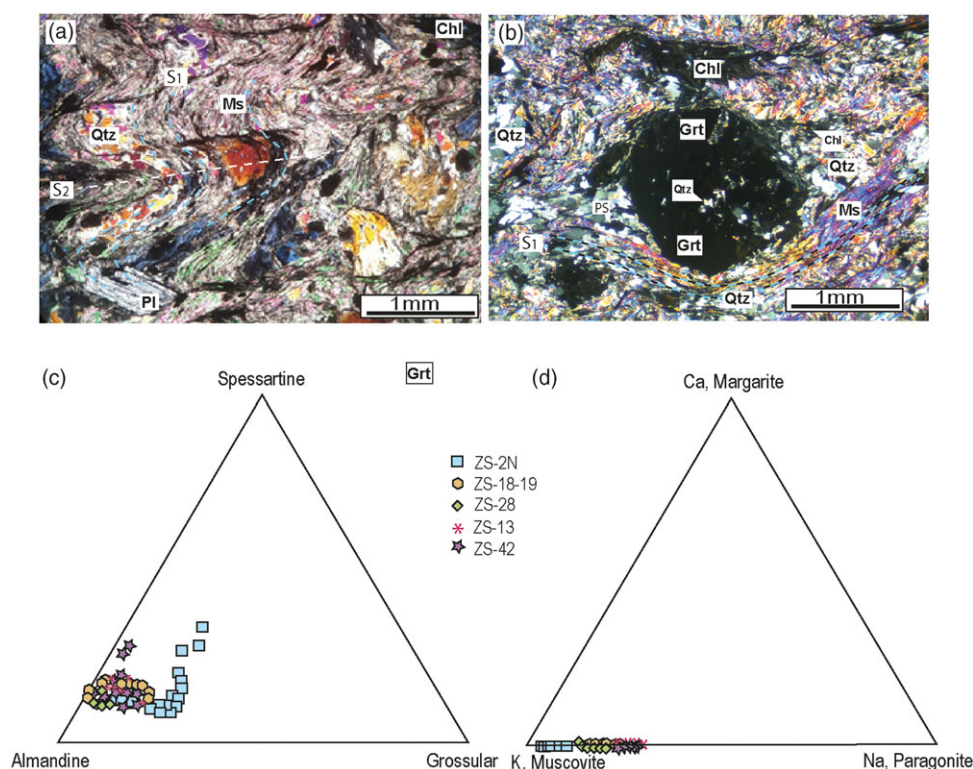


Fig. 4. (Colour online) (a) Foliation in muscovite schist. The main foliation (S_1) is folded by S_2 . (b) Garnet with pressure shadow structures in textural equilibrium with metamorphic chlorite (both in cross-polarized light). (c) Garnet composition in garnet schist (samples ZS-2N, ZS-18-19, ZS-28, ZS-13 and ZS-42) and gneiss (samples ZS-1-15 and ZS-1-12), which is almandine-rich. (d) Composition of plagioclase in the amphibolite samples. Plagioclases in sample ZS-3-B are albite to andesine, in sample ZS-1-14 are andesine and in sample ZS-43 they are albite to andesine.

into chlorite. Quartz, biotite, muscovite and garnet are the major phases and plagioclase, secondary chlorite, opaque minerals, tourmaline and zircon are the minor and accessory phases. The main lepidoblastic texture of the groundmass of this rock type is formed by parallel aligned mica flakes. The pervasive schistosity is deformed by secondary deformational phase, reflected by microfolds (Fig. 4a). Garnet porphyroblasts up to 2 mm across have inclusions of muscovite and quartz. They show symmetrical pressure shadows. Quartz is the main mineral in the shadow (Fig. 4b). Petrographical studies indicate retrograde changes of biotite and garnet into chlorite. Also chlorite is formed on the microfolds limbs and hinges of the second deformation (Fig. 4a). These observations testify for an amphibolite (formation of garnet and biotite) and overprinting greenschist (mainly chlorite formation) polyphase metamorphism for the studied rocks. Mineral compositions are relatively constant within individual samples but are relatively different among the studied samples. In the analysed samples, garnet is almandine-rich (Table 2) with formula of $\text{Alm}_{52.4-81.5}\text{Sp}_{0.9-26.1}\text{Grs}_{24.2-0.7}\text{Prp}_{1.2-14.7}$ (Fig. 4c). Garnet in sample ZS-2N, which is a semipelitic rock with high quartz content, shows the highest spessartine and the lowest almandine contents (Fig. 4c). Apart from this sample, garnet in other samples shows very limited variations in the major oxide contents across the crystals, indicating lack of significant chemical zoning. White mica is mainly muscovite-rich with considerable phengite and low paragonite end-member contents occasionally (Table 3). Margarite component was not recognized (Fig. 4d). No aluminosilicate polymorph was found in the Allahyarlu samples.

The fabric of the gneisses is defined by alternating mica- and garnet-rich and quartz-feldspar-rich layers, respectively. The main minerals are quartz, plagioclase, garnet, muscovite and biotite. The minor phases include chlorite, tourmaline, epidote, titanite and opaque minerals, and zircon is the accessory phase (Table 1). Graphite can be found in some samples. The main textures are granoblastic, formed by quartz and feldspar, within the microlithon domains of the rock and lepidoblastic formed by parallel mica flakes in the mica-rich parts of the rock, which compose the schistosity domains. Garnet (up to 3 mm across) appears as relatively large crystals with inclusions of biotite, muscovite and quartz. Muscovite flakes are relatively large (up to 1 mm) in some samples. Retrograde products are chlorite after biotite and garnet and sericite after feldspar. The ratio of quartz to other minerals is high, which along with the presence of graphite in some samples indicates a paragneiss nature for the studied samples. The chemistry of garnet and white mica is very close to those in the schists (Fig. 4a, b). Amphibolites can be divided into garnet-free and garnet-bearing varieties (Table 1). Hornblende and plagioclase are the main phases. Titanite, calcite, rare biotite, epidote, Fe-oxides and zircon constitute the minor and accessory phases. The main texture of the rocks is nematoblastic, formed by parallel alignment of the hornblende prisms (up to 4 mm long), making the rock lineation. This is the pervasive deformational phase in the amphibolite samples (Fig. 5a). In some samples fine-grained (<0.5 mm) quartz is present in low modal amounts. Garnets occur in garnet amphibolites as small grains (~0.5 mm) with inclusions of hornblende, plagioclase and Fe-oxides. Samples with garnet lack epidote.

Table 2. Representative garnet analyses in the studied rocks (Am: amphibolite; Sch: schist; Gns: gneiss). The formula unit is calculated based on 12 oxygen atoms

Samples	ZS-1-14, Am		ZS-2 N, Sch		SY18-9, Sch		ZS-28, Sch		ZS-13, Sch		ZS-42, Sch		Zs-1-12, Gns		Zs-1-15, Gns	
SiO ₂	37.74	37.95	36.57	36.59	37.24	36.74	36.11	35.94	36.02	36.50	37.31	37.41	37.38	36.92	37.13	37.09
TiO ₂	0.13	0.11	0.12	0.06	0.06	0.02	0.13	0.05	0.03	0.05	0.13	0.08	0.04	0.04	0.02	0.01
Al ₂ O ₃	21.69	21.84	20.75	20.97	21.05	21.19	21.10	20.98	20.91	21.13	21.31	21.53	21.50	21.38	21.26	21.34
Cr ₂ O ₃	0.01	0.00	0.00	0.00	0.04	0.02	0.03	0.00	0.00	0.05	0.01	0.01	0.00	0.00	0.01	0.01
FeO	27.01	27.01	23.03	26.88	32.57	35.00	34.95	36.18	34.97	34.36	33.15	32.73	32.61	33.28	31.86	31.82
MnO	2.66	1.13	11.31	8.19	1.48	2.97	1.30	1.97	1.67	1.59	0.78	0.82	1.54	2.33	2.14	2.03
MgO	2.64	3.26	0.31	0.35	3.09	2.49	2.23	2.24	2.95	3.08	3.62	3.75	3.57	2.78	3.11	3.16
CaO	8.87	9.64	6.92	6.39	3.94	1.44	3.10	1.73	2.29	2.45	3.55	3.67	3.40	3.18	3.77	3.78
Total	100.76	100.93	99.01	99.43	99.47	99.86	98.95	99.09	98.84	99.21	99.85	100.00	100.04	99.91	99.30	99.24
Si	2.97	2.96	2.99	2.98	3.00	2.98	2.95	2.94	2.93	2.96	2.98	2.98	2.98	2.97	2.99	2.99
Ti	0.01	0.01	0.01	0.00	0.00	0.00	0.01	0.00	0.00	0.00	0.01	0.00	0.00	0.00	0.00	0.00
Al	2.01	2.01	2.00	2.01	2.00	2.02	2.03	2.02	2.01	2.02	2.01	2.02	2.02	2.03	2.02	2.03
Cr	0.00	0.00	0.00	0.00	0.00	0.00	0.00	0.00	0.00	0.00	0.00	0.00	0.00	0.00	0.00	0.00
Fe ³⁺	0.03	0.05	0.00	0.01	0.00	0.02	0.06	0.09	0.12	0.06	0.01	0.01	0.00	0.00	0.00	0.00
Fe ²⁺	1.74	1.71	1.57	1.82	2.19	2.35	2.32	2.38	2.26	2.27	2.20	2.17	2.18	2.24	2.15	2.14
Mn	0.18	0.07	0.78	0.57	0.10	0.20	0.09	0.14	0.12	0.11	0.05	0.06	0.10	0.16	0.15	0.14
Mg	0.31	0.38	0.04	0.04	0.37	0.30	0.27	0.27	0.36	0.37	0.43	0.45	0.42	0.33	0.37	0.38
Ca	0.75	0.81	0.61	0.56	0.34	0.12	0.27	0.15	0.20	0.21	0.30	0.31	0.29	0.27	0.33	0.33
Alm	58.53	57.55	52.38	60.96	72.96	78.86	78.60	80.93	77.07	76.56	73.65	72.74	72.55	74.22	71.76	71.75
Sps	5.95	2.51	26.13	18.93	3.36	6.84	3.04	4.64	3.92	3.69	1.76	1.84	3.49	5.34	4.88	4.64
Prp	10.40	12.78	1.26	1.42	12.35	10.10	9.18	9.28	12.20	12.57	14.43	14.92	14.23	11.22	12.48	12.70
Grs	24.68	26.44	20.18	18.58	11.29	4.15	8.89	4.92	6.42	6.96	10.10	10.44	9.69	9.07	10.88	10.92

Rare quartz occurs along with plagioclase (up to 2 mm) as a light envelope wrapping the garnet crystals (Fig. 5b). Amphibole in amphibolites is calcic (Table 4) and shows a compositional range from ferro-tschermakite to magnesio-hornblende (Fig. 6a). Based on Na+K versus Si in the formula unit, amphibole compositions in samples ZS-1-14 and ZS-43 range from hornblende to tschermakite types, while amphibole in sample ZS-3-B ranges from edenite to pargasite (Fig. 6b). The garnet composition (Table 2) is Alm_{56.7-59.6}Sps_{1.3-6.2}Grs_{24.2-28.8}Pyp_{10-14.5} (Fig. 6c), and plagioclase ranges from pure albite to andesine (Table 5; Fig. 6d). Plagioclase composition in sample SZ-1-14 is An_{29.6-37.07}Ab_{61.2-69.92}Or_{0.0-0.8}, in sample ZS-3-B is An_{0.5-31.4}Ab_{68.0-99.2}Or_{0.0-0.6} and in sample ZS-43 is An_{3.4-33.6}Ab_{65.7-95.9}Or_{0.5-1.2}. Primary chlorites in textural equilibrium with garnet are Fe- and Mg-rich, with Fe varying from 1.38 to 2.24 in the formula unit (based on 14 oxygen atoms) while Mg number is from 1.64 to 2.31 atom per formula unit. Ca and Mn contents are negligible (Table 6).

5. Metamorphic P-T estimates

The P-T estimates based on different methods and calibrations indicate a relatively wide range of metamorphic conditions for the Allahyarlu metamorphic rocks. Since all studied rocks contain hydrous minerals such as muscovite, chlorite and amphibole, we assumed water saturation condition for the metamorphism. Pelitic rocks lack aluminosilicate polymorphs, which hinders

application of the most reliable thermobarometers for these rocks. In the amphibolites, there is no suitable mineral paragenesis that would allow determining pressure precisely. The rocks show no indications for partial melting. This suggests a maximum T limit for the metamorphism of c. 650 °C. Since metapelitic and metabasic rocks share similar structures and textures and are closely associated in the field, we consider it likely that they share the same metamorphic history.

5.a. Temperature estimates for garnet mica schists

Quartz, garnet, muscovite, plagioclase and chlorite are in textural equilibrium in the studied samples. Biotite is altered into chlorite. Due to the lack of suitable mineral paragenesis for pressure estimates in the pelitic rocks, nominal pressures are used to calculate temperature. Thermodynamic modelling and calibrations of the Grt–Ms thermometer were studied by Krogh & Raheim (1978), Green & Hellman (1982), Hynes & Frost (1988) and Wu *et al.* (2002). This thermometer is based on Fe–Mg exchange between muscovite and garnet in thermodynamic equilibrium and can be applied to rocks in the temperature range 480–700 °C and pressures of 3 to 14 kbar (Wu *et al.* 2002). It is applicable if the Mg content of muscovite is less than 0.13 and the Fe content is more than 0.04 atom per formula unit based on 11 oxygen atoms. Our samples meet these criteria (Tables 2, 3). The garnet solid solution model is from Holdaway (2000), and muscovite is treated as a symmetric Fe–Mg–Al^{VI} ternary solid solution. Wu & Zhao

Table 3. Representative muscovite analyses in the studied rocks (Sch: schist; Gns: gneiss). The formula unit is calculated based on 11 oxygen atoms

Samples	Zs-2 N, Sch		Zs-18-9, Sch		Zs-28, Sch		Zs-13, Sch		ZS-42, Sch		Zs-1-12, Gns		Zs-1-15, Gns	
SiO ₂	51.11	50.73	46.84	46.71	46.15	46.58	47.14	46.83	47.38	46.37	45.11	43.98	46.17	46.32
TiO ₂	0.32	0.34	0.12	0.36	0.77	0.71	0.62	0.52	0.25	0.27	0.44	0.42	0.34	0.29
Al ₂ O ₃	27.97	27.11	35.37	35.50	35.35	35.63	35.47	35.26	35.67	36.10	35.08	33.65	35.78	35.13
Cr ₂ O ₃	0.00	0.03	0.00	0.00	0.01	0.00	0.00	0.00	0.00	0.08	0.00	0.00	0.00	0.01
FeO	2.78	3.28	1.03	1.19	1.14	1.06	1.04	0.77	0.69	0.92	0.96	1.93	0.74	0.68
MnO	0.00	0.04	0.00	0.02	0.00	0.00	0.06	0.00	0.00	0.00	0.00	0.00	0.00	0.02
MgO	2.57	2.38	0.63	0.62	0.49	0.47	0.59	0.65	0.54	0.65	0.65	0.92	0.59	0.71
CaO	0.00	0.02	0.00	0.02	0.04	0.01	0.03	0.02	0.01	0.00	0.05	0.01	0.00	0.00
Na ₂ O	0.34	0.32	1.59	1.57	1.59	1.37	1.96	1.81	2.04	2.07	1.34	1.93	1.71	1.70
K ₂ O	10.71	10.31	9.16	9.00	8.62	9.24	8.65	8.61	8.49	8.85	9.74	7.94	8.72	8.78
Total	95.81	94.58	94.75	95.01	94.17	95.06	95.56	94.47	95.07	95.32	93.39	90.91	94.05	93.66
Si	3.37	3.39	3.10	3.09	3.07	3.08	3.09	3.10	3.12	3.06	3.05	3.05	3.08	3.10
Ti	0.02	0.02	0.01	0.02	0.04	0.04	0.03	0.03	0.01	0.01	0.02	0.02	0.02	0.01
Al	2.18	2.14	2.76	2.77	2.77	2.77	2.74	2.75	2.76	2.81	2.80	2.75	2.81	2.77
Cr	0.00	0.00	0.00	0.00	0.00	0.00	0.00	0.00	0.00	0.00	0.00	0.00	0.00	0.00
Fe ²⁺	0.15	0.18	0.06	0.07	0.06	0.06	0.06	0.04	0.04	0.05	0.05	0.11	0.04	0.04
Fe ³⁺	0.00	0.00	0.00	0.00	0.00	0.00	0.00	0.00	0.00	0.00	0.00	0.00	0.00	0.00
Mn	0.00	0.00	0.00	0.00	0.00	0.00	0.00	0.00	0.00	0.00	0.00	0.00	0.00	0.00
Mg	0.25	0.24	0.06	0.06	0.05	0.05	0.06	0.06	0.05	0.06	0.07	0.09	0.06	0.07
Ca	0.00	0.00	0.00	0.00	0.00	0.00	0.00	0.00	0.00	0.00	0.00	0.00	0.00	0.00
Na	0.04	0.04	0.20	0.20	0.21	0.18	0.25	0.23	0.26	0.26	0.18	0.26	0.22	0.22
K	0.90	0.88	0.77	0.76	0.73	0.78	0.72	0.73	0.71	0.74	0.84	0.70	0.74	0.75
Mg/(Mg + Fe ²⁺ + Mn)	1.00	0.99	1.00	0.98	1.00	1.00	0.94	1.00	1.00	1.00	1.00	1.00	1.00	0.99
Fe ²⁺ /(Mg + Fe ²⁺ + Mn)	0.00	0.00	0.00	0.00	0.00	0.00	0.00	0.00	0.00	0.00	0.00	0.00	0.00	0.00
Na/(Na + K)	0.05	0.05	0.21	0.21	0.22	0.18	0.26	0.24	0.27	0.26	0.17	0.27	0.23	0.23

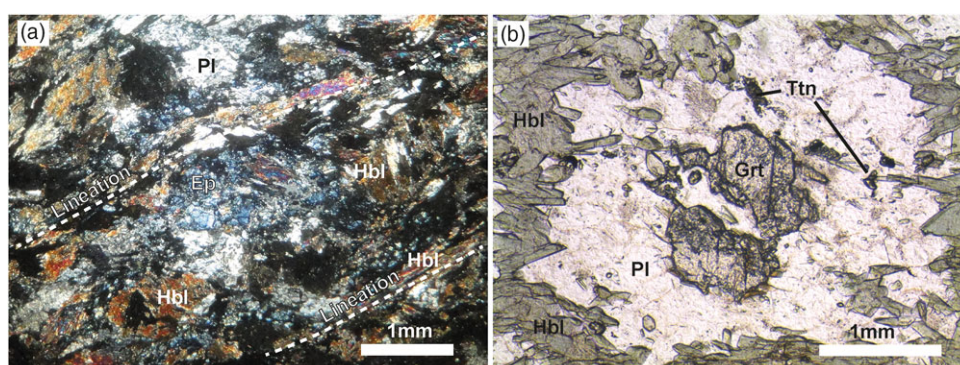


Fig. 5. (Colour online) Photomicrographs of (a) amphibolite and (b) garnet amphibolite from the Allahyarlu area (both in plain polarized light).

(2006) proposed two equations for temperature calculations, one for garnet without ferric iron and another for garnet with 50 % ferric iron. An asymmetric Quaternary solid solution is considered for garnet in the calibration. The studied garnets do not have considerable ferric iron in their compositions, therefore we have used model (A) of Wu *et al.* (2002). Temperatures are estimated for two samples for nominal pressures of 2 to 9 kbar. The core

compositions of garnet are used. The range of temperature is 506 to 558 °C, with an average of 532 °C. Wu *et al.* (2002) consider a ± 5 °C uncertainty for this thermometer. Chlorite appears both as replacing garnet and biotite and as relatively large flakes parallel to the main foliation (Fig. 4a). The composition of the second type of chlorite, considered to be in equilibrium with garnet, is used for temperature calculations using the Grt–Chl thermometer. This

Table 4. Representative amphibole analyses in the studied rocks (Grt Am: garnet amphibolite; Am: amphibolite). The formula unit is calculated based on 13 cations (CaNaK) and 23 oxygen atoms

Samples	ZS-1-14, Grt Am		ZS-3B, Am		Zs-X43, Am	
SiO ₂	41.54	41.98	39.83	43.33	45.26	45.09
TiO ₂	0.53	0.61	0.57	0.42	0.48	0.59
Al ₂ O ₃	16.64	16.06	13.57	11.68	12.08	12.07
FeO	16.05	16.71	20.59	19.25	16.53	16.28
MnO	0.27	0.26	0.29	0.31	0.25	0.29
MgO	7.84	8.13	7.39	8.57	9.62	9.57
CaO	10.96	11.42	10.93	10.34	11.62	11.54
Na ₂ O	1.32	1.25	3.15	2.75	1.12	1.31
K ₂ O	0.63	0.55	0.34	0.26	0.57	0.73
Cr ₂ O ₃	0.00	0.00	0.00	0.01	0.03	0.15
NiO	0.05	0.00	0.00	0.01	0.00	0.00
Total	98.28	99.47	99.14	99.50	99.96	100.02
Si	6.21	6.22	6.11	6.51	6.67	6.66
Al ^{iv}	1.79	1.78	1.89	1.49	1.33	1.34
Al	2.93	2.81	2.45	2.07	2.10	2.10
Al ^{vi}	1.15	1.03	0.56	0.57	0.76	0.76
Ti	0.06	0.07	0.07	0.05	0.05	0.07
Cr	0.00	0.00	0.00	0.00	0.00	0.02
Fe ³⁺	0.51	0.52	0.60	0.64	0.36	0.25
Fe ²⁺	1.50	1.55	2.05	1.77	1.67	1.76
Mn	0.03	0.03	0.04	0.04	0.03	0.04
Mg	1.75	1.80	1.69	1.92	2.11	2.11
Ni	0.01	0.00	0.00	0.00	0.00	0.00
Ca	1.76	1.81	1.80	1.66	1.83	1.83
Na	0.38	0.36	0.94	0.80	0.32	0.37
K	0.12	0.10	0.07	0.05	0.11	0.14

thermometer is based on the Fe–Mg exchange between chlorite and garnet in the presence of quartz (Dickinson & Hewitt, 1986; Ghent *et al.* 1987; Grambling, 1990). We used the calibration by Grambling (1990), with an assumed ± 8 °C uncertainty. Nominal pressures of 3, 4, 6 and 8 kbar are used for T calculations. Due to limited pressure dependence of this method (Grambling, 1990), the calculated temperatures for different pressures are identical. The T range is 525–586 °C with an average of ~ 556 °C. This temperature is similar to T estimates from the Grt–Ms thermometry above, indicating lower amphibolite facies peak metamorphic conditions. To estimate the peak P – T conditions of the pelitic rocks, sample ZS-13 with the highest Al₂O₃ content (more pelitic than psammitic) was used for calculation by the pseudosection method by means of the Domino/Theriak software (De Capitani & Brown, 1987) in the MnCN-KFMASH system. The internally consistent dataset of Berman (1988) was used for the calculations. The pseudosection is shown in Figure 7a. Grt + Chl + Pl and Grt + Chl + Bt fields on the pseudosection are narrow, considering the temperature changes. Muscovite content in white mica (Fig. 7b), and almandine content in garnet (Fig. 7c) are calculated. Based on EPMA, the white mica muscovite

content is 0.74 mole %, and the garnet almandine content is 0.76 mole %. These isopleths are intersected in two points (Fig. 7d), indicating a temperature and pressure range for metamorphism (stars in Fig. 7a, d). Pressure of 4.5–5 kbar and temperature of $c.$ 530–570 °C can be considered for peak metamorphism of the pelitic samples using these diagrams.

5.b. P – T estimates for the amphibolites

Hornblende, garnet and plagioclase are the main minerals in textural equilibrium in the amphibolites. Several thermobarometers are applied to these rocks. Hornblende–plagioclase (Hbl–Pl) thermometer (Blundy & Holland, 1990; Schmidt, 1992; Blundy & Holland, 1994; Stein & Dietl, 2001) is calibrated based on edenitic and tschermakitic substitutions in amphibole. Blundy & Holland (1994) calibrated this thermometer with edenite + albite = richterite + anorthite and edenite + quartz = tremolite + albite reactions. Since quartz is absent or occurs in very low amounts in our amphibolite samples, we have used the quartz-free version of the thermometer (Blundy & Holland, 1994). The range of temperature for three samples is 601 to 862 °C. Samples ZS-1-14 and

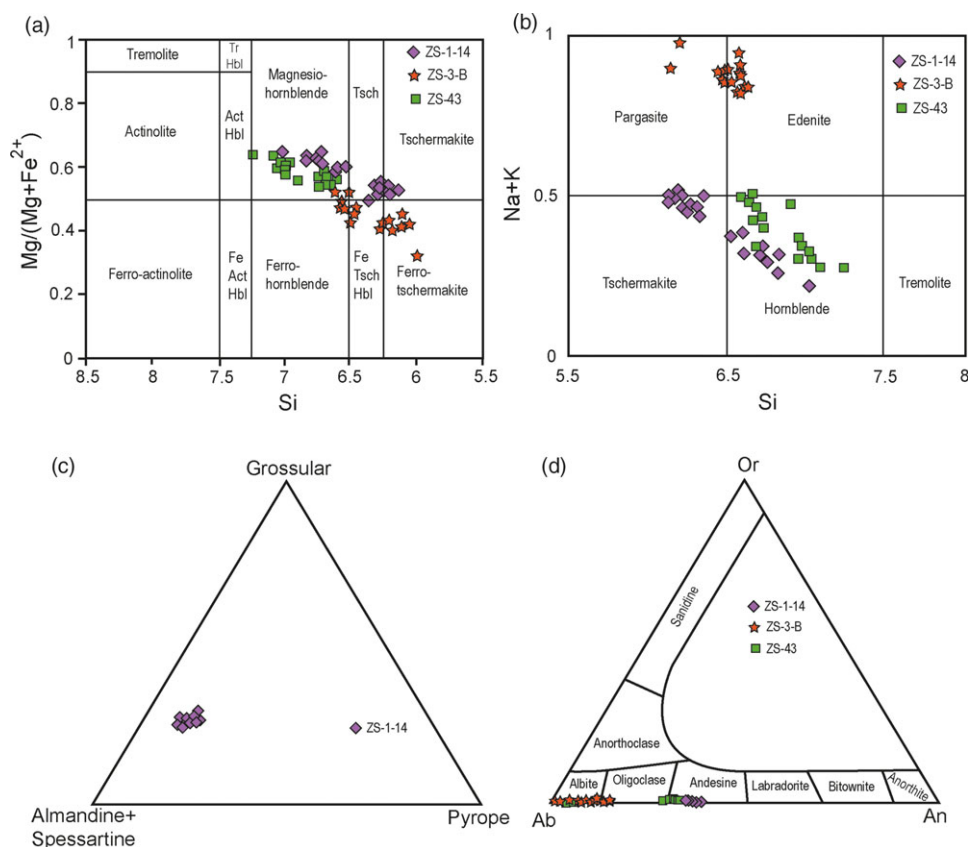


Fig. 6. (Colour online) Composition of amphibole (a, b), garnet (c) and feldspar (d) in the studied amphibolites.

SZ-3B show relatively higher temperatures. Titanite is present in the studied amphibolite samples. This shows that Ti was saturated in the rock systems and Ti content in hornblende is mainly controlled by temperature (Raase, 1974; Ernst & Liu, 1998). Ti in Hbl thermometry of Otten (1984) was used to further constrain the metamorphic temperature of the amphibolite samples. This thermometer is *P*-independent and gives temperatures of 581–617 °C. Grt–Pl thermometry (Graham & Powell, 1984; Perchuk *et al.* 1985) gives temperatures of 513 to 581 °C, and Grt–Hbl thermometer (Krogh, 2000) indicates 600 °C for garnet amphibolite metamorphism. Pressure estimates for the Allahyarlu amphibolites are problematic owing to the lack of suitable mineral paragenesis. We consider a pressure of *c.* 5 kbar estimated from the pelitic rocks as realistic for the amphibolites, since the two rock types occur together in the field, showing similar deformation and metamorphic events, but this might be a minimum estimate owing to the presence of garnet in this lithology. The range of temperature estimated for the pelitic rocks in the area is 505–586 °C for different samples. These temperatures are close considering the uncertainties in the *T* estimation. Temperatures estimated for the amphibolites are at the same range (513–670 °C). We regard the highest temperatures from the Hbl–Pl calibration for samples ZS-1-14 and ZS-3B as unrealistic, since these temperatures correspond to the granulite facies, while no granulite facies minerals (e.g. orthopyroxene) have been found in the studied samples. Based on thermobarometry results for both mafic and pelitic rocks, an average pressure of *c.* 5 kbar and an average temperature of *c.* 600 °C can be considered for the metamorphism in the Allahyarlu complex. Considering an average density of 2700 kg m⁻³ for the upper crustal rocks, a lithostatic pressure of

1 kbar corresponds to depth of burial of ~3.75 km. An average pressure of 5 kbar for the Allahyarlu metamorphic rocks is therefore equivalent to ~18 km depth of burial. Taking 600 °C as the average temperature, the geothermal gradient for the area was ~33 °C km⁻¹ during metamorphism, which might develop in response to a collisional context in the continental crust or to a thick magmatic arc setting (e.g. Jamieson *et al.* 1998).

The results for *P–T* estimates on the studied rocks are summarized in Table 7.

6. Amphibolite whole rock chemistry

Eight representative amphibolite samples were analysed for major and trace elements (Table 8). SiO₂ contents of the analysed samples form a very narrow range from 49.1 to 51.3 wt %. Al₂O₃ contents are 13.74–15.31 wt %, and MgO varies from 5.1 to 7.33 wt %. The Fe₂O₃ (total) content is 9.16–10.26 wt %. These chemical features point to a mafic (basaltic) composition of the protolith. TiO₂ content of the rocks is 1.30–1.85 wt %, Na₂O content is 2.14–3.01 wt %, while K₂O content is 0.49–0.90 wt %. Considering the whole rock geochemistry of the studied amphibolites, relatively high TiO₂, MgO and Fe₂O₃ (total) contents versus very low K₂O and low SiO₂ contents may testify for an igneous (ortho-amphibole) nature of the protolith (e.g. Moghazi *et al.* 2001). We have used the whole rock chemistry of the amphibolite samples to constrain the nature of the magmatic series and the tectonic setting of the protolith. Immobile and relatively mobile elements during greenschist to amphibolite facies metamorphism (Pearce & Cann, 1973; Coish, 1977; Floyd & Winchester, 1978; Rollinson, 1993) are used in this regard. The results from these

Table 5. Representative plagioclase analyses in the studied amphibolite samples (Grt Am: garnet amphibolite; Am: amphibolite). The formula unit is calculated based on 8 oxygen atoms

Samples	Zs-1-14, Grt Am		Zs-3B, Am		Zs-43, Am	
SiO ₂	59.48	58.23	65.79	69.20	60.75	68.41
TiO ₂	0.00	0.10	0.00	0.00	0.15	0.00
Al ₂ O ₃	25.16	25.81	21.23	18.99	24.72	20.02
Cr ₂ O ₃	0.05	0.00	0.00	0.04	0.00	0.00
MnO	0.00	0.05	0.04	0.03	0.00	0.00
MgO	0.00	0.03	0.03	0.02	0.00	0.00
CaO	6.72	7.99	2.28	0.22	6.63	0.72
Na ₂ O	7.86	7.01	10.05	12.32	7.94	11.11
K ₂ O	0.12	0.05	0.04	0.04	0.11	0.12
Total	99.41	99.36	99.87	101.25	100.36	100.67
Si	2.66	2.62	2.91	2.98	2.70	2.98
Ti	0.00	0.00	0.00	0.00	0.01	0.00
Al	1.33	1.37	1.11	0.96	1.29	1.03
Ca	0.32	0.39	0.11	0.01	0.32	0.03
Na	0.68	0.61	0.86	1.03	0.68	0.94
K	0.01	0.00	0.00	0.00	0.01	0.01
An	31.87	38.53	11.11	0.99	31.38	3.41
Ab	67.45	61.17	88.64	98.79	68.00	95.92
Or	0.68	0.31	0.25	0.22	0.62	0.67

two types of elements are comparable. The studied samples are enriched in large-ion lithophile elements (LILE) compared to high field strength elements (HFSE). Ta, Nb, P and Ti (all HFSE) show negative anomalies, and heavy rare earth elements (HREE) contents show negligible variation.

7. The age of metamorphism

Muscovite separated from two gneiss samples (ZS-1-12 and ZS-15) and hornblende separated from three amphibolite samples (ZS-3b, ZS-43a and ZS-43b) were used for ⁴⁰Ar–³⁹Ar dating. The resulting data are provided in the Appendix.

7.a. Sample ZS-1-12, muscovite

This sample is well defined by a 12-step spectrum. The central portion of the spectrum representing more than 91 % of the released ³⁹Ar gives a well-defined plateau age of 333.7 ± 0.8 Ma. The isochron correlation gives slightly older age (338.2 ± 2.0 Ma), and the inverse isochron shows a similar within-error age (334.5 ± 1.3 Ma) to the plateau age (Fig. 8). Therefore, given the very homogeneous behaviour of this sample, it is in good agreement with a crystallization of the muscovite at c. 334 Ma. The total fusion age of the sample is also similar within error (338 ± 0.3 Ma), pointing to a very low alteration for this sample.

7.b. Sample ZS-15, muscovite

This sample also shows a homogeneous spectrum, and a well-defined plateau age with ten heating steps. The central portion of

Table 6. Representative chlorite analyses in the studied garnet schist samples. The formula unit is calculated based on 14 oxygen atoms

Sample	ZS-42			ZS-13		
SiO ₂	23.73	23.64	25.34	34.89	35.89	29.02
TiO ₂	0.07	0.11	0.13	1.23	1.83	0.66
Al ₂ O ₃	22.93	22.89	22.42	19.38	20.11	18.41
Cr ₂ O ₃	0.02	0.03	0.08	0.03	0.04	0.02
FeO	24.93	24.03	25.34	17.64	16.55	23.02
MnO	0.01	0.05	0.09	0.02	0.03	0.08
MgO	14.14	14.32	13.72	11.60	11.03	13.03
CaO	0.00	0.00	0.00	0.05	0.03	0.52
Total	85.83	85.08	87.29	84.84	85.50	84.76
Si	2.55	2.56	2.68	3.54	3.58	3.10
Ti	0.01	0.01	0.01	0.09	0.14	0.05
Al	2.91	2.92	2.80	2.32	2.36	2.32
Cr	0.00	0.00	0.01	0.00	0.00	0.00
Fe ²⁺	2.24	2.17	2.24	1.50	1.38	2.06
Mn	0.00	0.00	0.01	0.00	0.00	0.01
Mg	2.27	2.31	2.16	1.75	1.64	2.08
Ca	0.00	0.00	0.00	0.01	0.00	0.06
Total	9.98	9.97	9.91	9.21	9.10	9.68
Mg/(Mg + Fe)	0.50	0.52	0.49	0.54	0.54	0.50
Fe/(FeMnMg)	0.48	0.49	0.47	0.52	0.55	0.44
Mg/(FeMnMg)	0.52	0.51	0.53	0.48	0.45	0.56

the spectrum, representing 96.6 % of the released ³⁹Ar, gives a plateau age of 324.0 ± 0.8 Ma. The total fusion age of this sample is of 323.6 ± 0.2 Ma, which is similar within-error to the plateau age (Fig. 8). The isochron correlations also correspond very well with this age (normal isochron age 324.0 ± 1.3 Ma; inverse isochron age 323.0 ± 1.9 Ma). Therefore, given the consistency of the released Ar–Ar signal in this sample, we interpret this age as a geologically meaningful age, which corresponds to the crystallization of the muscovite at c. 326 Ma.

7.c. Sample ZS-3b, hornblende

This sample gave eight heating steps. It shows a bell-shape Ar release pattern starting with lower ages (c. 93 Ma) and culminating at ages of 323–325 Ma in the central part of the Ar–Ar spectrum. Thus, this sample shows a more complex thermal history than the muscovites. Initial crystallization age was partly preserved in the core of the grain, as emphasized by similar Ca/K ratios obtained by EPMA in amphibole core and in 323–325 Ma age steps by spectrometric analysis (Fig. 9). These high Ca/K ratios correspond to the higher temperature steps apart from the melting step, which still preserved a younger age component and a lower Ca/K ratio. The lower step ages are in agreement with a mixture of amphibole with a <100 Ma phyllosilicate, as shown by Ca/K ratios which appear to be lower than amphibole rims (Ca/K = 24). Therefore, these ages are regarded as mixed ages with no geological significance. The two older steps agree with a minimum age of 325 Ma, close to the age of the high-temperature

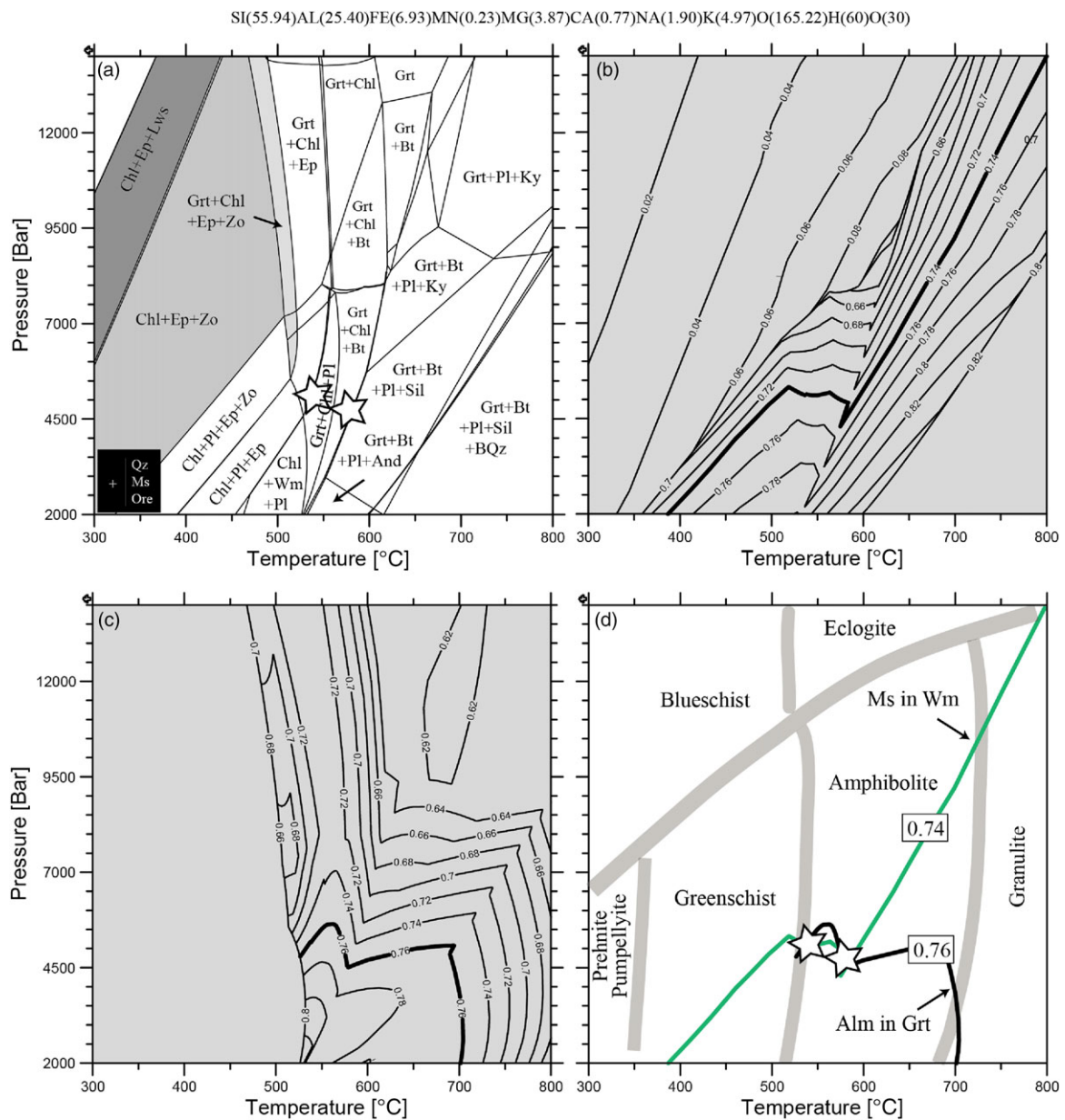


Fig. 7. (Colour online) (a) Pseudosections for one pelitic schist (ZS-13); (b, c) calculated isochems for muscovite (b) and almandine (c) contents in the minerals; (d) intersection of muscovite in white mica isochem of 0.74 mole % and almandine in garnet isochem of 0.76 mole % indicates pressure of c. 4.5 kbar and temperature of 530 to 570 °C.

metamorphic amphibole. The lower-temperature steps correspond to the contribution of some small alteration phases due to a recrystallization stage with a maximum age of 93 Ma.

The age pattern of amphiboles is not due to a core–rim variation towards actinolite. If this was the case, the corresponding Ca/K ratios would be much higher, as actinolite has higher Ca/K ratio than hornblende. Besides, actinolite has a very low K content and generally contains very little argon.

7.d. Sample ZS-43, hornblende

The Ar release pattern of this sample is similar to that of sample ZS-3b, with ten steps. It shows a bell shape starting with lower ages (minimum c. 122 Ma) and culminating at an age of 288 Ma

in the central part. Thus, this sample also indicates a complex thermal and crystallization history. As for sample ZS-3b, a correlation is found in the Ca/K versus age plot, highlighting a tendency towards higher Ca/K ratios in the higher age steps (Fig. 9). However, the highest Ca/K values are still lower than the values analysed by EPMA. Thus the step age of 288 Ma is interpreted as a minimum age for the initial metamorphic growth of the amphibole, and appears to have been significantly lowered in this sample by the contribution of high-K phase similar to sample ZS-3b. Extrapolating the ages to the corresponding EPMA values returns an age of ~350 Ma, which is coherent with the minimum age of sample ZS-3b amphibole. Accordingly, this sample has been strongly altered and recrystallized during a second event, with a maximum age of c. 122 Ma.

Table 7. Pressure–temperature estimates for the garnet schist and amphibolite samples

ZS-13		ZS-42	
Grt-MS , Wu <i>et al.</i> (2002)			
$T_{(A)} \text{ (K)} = 969.9 + P \text{ (kbar)} (1.3-9.1\text{Gb}) - 0.0091\text{Gc} - 4393.8(X_{\text{Fe}}^{\text{mus}} - X_{\text{Mg}}^{\text{mus}}) + 200.4X_{\text{Al}}^{\text{mus}} - 1 + 0.0091(3R \ln K_d + \text{Ga})$			
$P = 2 \text{ T, } = 506 \text{ }^\circ\text{C}$		$P = 2, T = 552 \text{ }^\circ\text{C}$	
$P = 3, T = 525 \text{ }^\circ\text{C}$		$P = 4, T = 553 \text{ }^\circ\text{C}$	
$P = 4, T = 515 \text{ }^\circ\text{C}$		$P = 5, T = 554 \text{ }^\circ\text{C}$	
$P = 5, T = 520 \text{ }^\circ\text{C}$		$P = 6, T = 555 \text{ }^\circ\text{C}$	
$P = 6, T = 553 \text{ }^\circ\text{C}$		$P = 9, T = 558 \text{ }^\circ\text{C}$	
$P = 9, T = 539 \text{ }^\circ\text{C}$			
Garnet-chlorite-quartz , Grambling (1990)			
$0 = 0.05P \text{ (bar)} - 19.02T \text{ (K)} + 4607 \ln k_D + 24.156$			
$P = 3-8 \text{ kbar, } T = 525 \text{ }^\circ\text{C}$		$P = 3-8 \text{ kbar, } T = 586 \text{ }^\circ\text{C}$	
ZS-1-14	ZS-3B	ZS-43	
Grt-amphibolite	Amphibolite	Amphibolite	
Grt-Plg			
Graham & Powell (1984)			
$T = 580 \text{ }^\circ\text{C}$			
Perchuk <i>et al.</i> (1985)			
$T = 513 \text{ }^\circ\text{C}$			
Grt-Hbl , Krogh (2000)			
$T = 600 \text{ }^\circ\text{C}$			
Hbl-Plg $P = 3 \text{ kbar}$ Blundy & Holland (1990) $T = 862 \text{ }^\circ\text{C}$	Amp-Plg $P = 3 \text{ kbar}$ Blundy & Holland (1990) $T = 800 \text{ }^\circ\text{C}$	Amp-Plg $P = 3 \text{ kbar}$ Blundy & Holland (1990) $T = 601 \text{ }^\circ\text{C}$	
Hbl-Plg $P = 5 \text{ kbar}$ Blundy & Holland (1990) $T = 829 \text{ }^\circ\text{C}$	Amp-Plg $P = 5 \text{ kbar}$ Blundy & Holland (1990) $T = 769 \text{ }^\circ\text{C}$	Amp-Plg $P = 5 \text{ kbar}$ Blundy & Holland (1990) $T = 670 \text{ }^\circ\text{C}$	
Ti in Amp , Otten (1984)			
$T = 617 \text{ }^\circ\text{C}$	$T \text{ (}^\circ\text{C)} = 581$	$T \text{ (}^\circ\text{C)} = 605$	
Geobarometer			
Grt-Amp-Plg			
$T = 600 \text{ }^\circ\text{C}$			
Kohn & Spear (1989) Amp model 1			
$P \text{ (kbar)} = 11.64 \ln kd\text{-Mg} = -5.904$			
$P \text{ (kbar)} = 7.73 \ln kd\text{-Fe} = -1.514$			
Kohn & Spear (1989) Amp model 2			
$P \text{ (kbar)} = 12.61 \ln kd\text{-Mg} = -3.560$			
$P \text{ (kbar)} = 6 \ln kd\text{-Fe} = 1.292$			
Kohn & Spear (1990)			
$P \text{ (kbar)} = 9.02 \ln kd\text{-Mg} = -0.810$			
$P \text{ (kbar)} = 9.55 \ln kd\text{-Fe} = 9.55$			

7.e. Sample ZS-43b, hornblende (ZS-43 duplicate)

This experiment revealed similar Ar–Ar spectra to the previous sample. As above, the highest age step also preserves the highest Ca/K ratio (Ca/K = 33), and thus the corresponding age of 283 Ma is a minimum age for the initial metamorphic growth of the muscovite. The recrystallization and/or retrograde of this mineral is shown by the contribution of a younger component with lower Ca/K ratios contribution, with a maximum age of 120 Ma (Fig. 9). According to the Ca/K ratios versus age plot, an initial age of 320–330 Ma could be hypothesized, which falls exactly within the range of muscovite plateau ages and of the maximum sample ZS-3b amphibole age. Based on the above ages, the main

metamorphic event recorded in the Allahyarlu metamorphic rocks is well defined by muscovite, which has been less severely altered than the amphiboles. The muscovite provides ages in the range 326–334 Ma. This is the minimum closure age but the maximum age on the spectrum. This age is similar to the minimum age of sample ZS-3b hornblende, suggesting contemporaneous crystallization of amphibole and muscovite during the HT peak. Ages younger than 120 Ma (sample ZS-X43) and 93 Ma (sample ZS-3b) can be attributed either to partial resetting of amphibole during a retrograde event or a mixture of different reservoirs for argon. This episode could be responsible for the widespread greenschist facies changes observed in the samples.

Table 8. Whole-rock chemistry of the amphibolite samples. Major oxides in mass % and the trace and rare earth elements in ppm

Sample	AZ-18-14	AZ-18-11	AZ-18-18	AZ-18-9	AZ-18-13	AZ-18-19	ZS-43	ZS-1-13
Rock type	(Grt Amp)	(Ep Amp)	(Grt Amp)	(Grt Amp)	(Grt Amp)	(Amp)	(Amp)	(Grt Amp)
SiO ₂	51.14	50.12	51.3	50.88	50.4	51.15	49.61	50.26
TiO ₂	1.74	1.55	1.85	1.75	1.714	1.63	1.30	1.66
Al ₂ O ₃	14.14	14.23	14.07	13.91	14.38	13.74	14.76	15.31
Fe ₂ O _{3T}	13.2	13.41	13.46	13.27	13.76	13.03	12.34	11.98
MnO	0.166	0.136	0.199	0.202	0.244	0.196	0.19	0.18
MgO	5.39	5.84	5.1	5.26	5.55	5.19	7.33	6.62
CaO	8.21	8.11	8.81	8.94	9.36	8.33	9.98	9.99
Na ₂ O	2.14	2.3	2.97	2.66	2.16	3.01	2.89	2.59
K ₂ O	0.7	0.8	0.9	0.81	0.7	0.83	0.75	0.49
P ₂ O ₅	0.13	0.14	0.15	0.11	0.09	0.14	0.09	0.18
LOI	3.45	3.21	1.55	1.32	1.14	1.65	1.49	1.06
Total	100.41	99.85	100.36	99.11	99.49	98.89	100.73	100.30
Sc	41	38	44	42	44	39	47	45
V	456	404	408	420	459	398	364	347
Ba	112	106	130	111	127	95	88	62
Sr	132	135	139	141	137	146	200	218
Y	28	33	32	34	29	32	31	33
Zr	70	75	87	73	69	88	67	115
Cr	60	58	60	65	60	80	94	142
Co	40	39	42	40	41	38	46	40
Ni	30	40	30	30	30	50	75	53
Cu	120	166	48	79	140	40	26	29
Zn	144	118	163	95	100	120	99	95
Rb	18	19	17	19	17	21	18	15
Nb	< 1	1	1	1	< 1	1	0.6	3.1
La	3.3	3.4	3.7	3.6	3.4	3.4	3.2	5.9
Ce	10.2	9.8	10.1	9.7	9.4	10.4	8.1	15.9
Pr	1.9	1.7	1.8	1.4	1.6	1.8	1.5	2.5
Nd	8.1	9.3	9.2	9.4	8.9	10.3	8.2	12.8
Sm	4	3.7	3.6	4	3.2	4	3	3.9
Eu	1.2	1	1	1.1	1.1	1.3	1.2	1.4
Gd	4.4	4.6	5.2	4.8	4.5	5.4	4.4	5.1
Tb	1	0.8	0.8	0.9	0.8	1	0.8	0.9
Dy	5.9	5.5	6.3	5.7	5.4	6.4	5.4	5.8
Ho	1.2	1.3	1.1	1.3	1.1	1.4	1.2	1.2
Er	3.4	3.6	3.7	3.5	3.5	4	3.5	3.6
Yb	3.7	3.6	3.8	3.5	3.5	3.9	3.4	3.3
Lu	0.6	0.6	0.6	0.6	0.5	0.6	0.5	0.5
Hf	2.1	2.2	2.1	2.2	1.9	2.3	2.1	2.9
Ta	0.1	0.1	0.1	0.1	0.1	0.1	0.1	0.2
Tl	0.1	0.1	0.1	0.1	< 0.1	0.1	0.1	0.1
Pb	5	5	< 5	5	5	< 5	5.4	4.3
Th	0.3	0.4	0.3	0.4	0.5	0.1	0.1	0.8
U	0.4	0.3	0.3	0.4	0.4	0.3	0.1	0.4

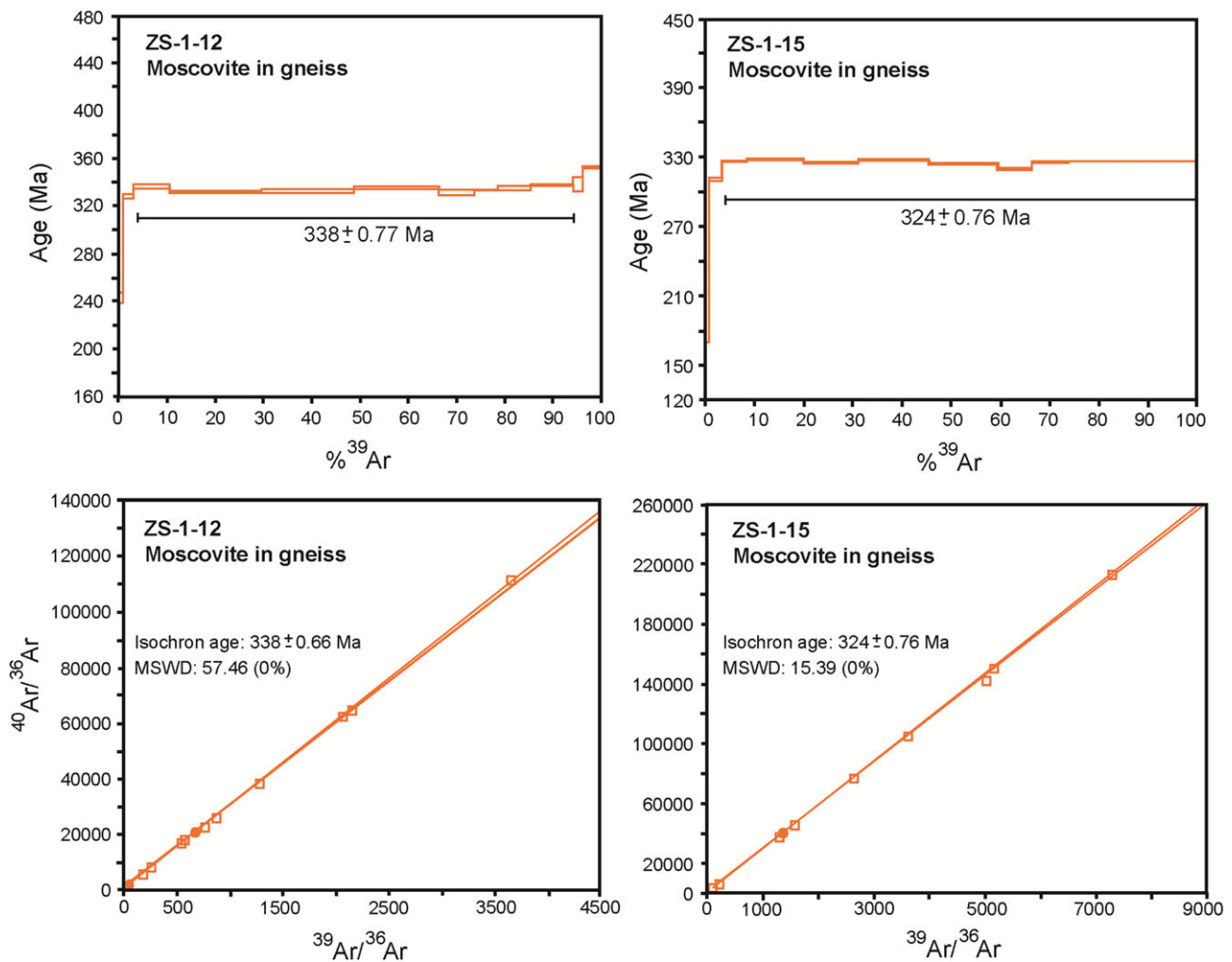


Fig. 8. (Colour online) ^{39}Ar - ^{40}Ar plateau ages (c. 325 and 338 Ma) for muscovite separates from the gneiss samples.

8. Discussion and conclusions

In order to find the nature of the protolith for the amphibolites, major oxides and trace elements are used. All samples plot in the igneous protolith or ortho-amphibolite fields in diagrams of $\text{Na}_2\text{O}/\text{Al}_2\text{O}_3$ versus $\text{K}_2\text{O}/\text{Al}_2\text{O}_3$ (Garrels & Mackenzie, 1971), MnO versus TiO_2 (Werner, 1987), MgO - CaO - FeO (Walker *et al.* 1959) and Zr versus MgO (Irvine & Baragar, 1971) in Figure 10 (all Fe is considered as FeO). Considering an igneous origin for the amphibolite protolith, the original magma type is characterized. The amphibolite samples with SiO_2 contents of 49.61 to 51.15 wt % and $\text{N}_2\text{O} + \text{K}_2\text{O}$ of 2.84 to 3.64 are similar to gabbro and gabbro-diorite or basalt and basaltic andesite in composition (Fig. 11a). The parental magma of the amphibolite protolith was metaluminous with a tholeiitic nature (Fig. 11b, c and d). It is similar to oceanic basalt (Fig. 12a), with tholeiitic composition transitional between mid-oceanic and island arc basalt (Fig. 12b, c, d). Rb, Hf, Ta and Th contents of the studied samples indicate an island arc setting for the protolith (Fig. 12e and f). V and Ti contents in mafic rocks are proxies to discriminate between different tectonic settings of mafic magmatism (Shervais, 1982). Vanadium has three oxidation states, which are stable in reduced (V^{3+}) and oxidized (V^{4+} and V^{5+}) conditions, while Ti can be found only as Ti^{4+} in magma. Therefore variation of

V concentrations against Ti concentrations is indicative of oxygen fugacity changes in magma. Shervais (1982) showed that a Ti versus V diagram can discriminate tholeiites formed in relation to an arc, mid-ocean ridge basalt (MORB) and ocean island basalts. Also this diagram allows discriminating fore-arc and back-arc basin basalts. The reason for this is that the crystal/liquid partitioning coefficient for V varies with oxygen fugacities from >1 to $<<1$. According to Pearce & Cann (1971, 1973), the f_{O_2} for magmas formed in the oceanic environment increases in the order island arcs $>$ back-arc basins $>$ ocean islands $>$ MORB. Discrimination diagrams involving Ti, V, Zr, Th and Co are used to distinguish the tectonic setting for the parental rocks of the amphibolites (Fig. 13). The samples plot within or close to the back-arc basin basalt fields in these diagrams. Trace element compositions of the samples are plotted on spider diagrams normalized to normal (N-) MORB (normalizing values are from Sun & McDonough, 1989). The studied samples show distinct positive anomalies in Rb, K and Pb and negative anomalies in Th, Nb, Ta (TNT) (Fig. 14a). These features clearly show a subduction-related system for the formation of the protolith of the amphibolites. The spider patterns are compared with a typical enriched and depleted back-arc basin basalt (Fig. 14a) and typical island arc basalt (island arc basalts in Guguan, Mariana arc; Pearce

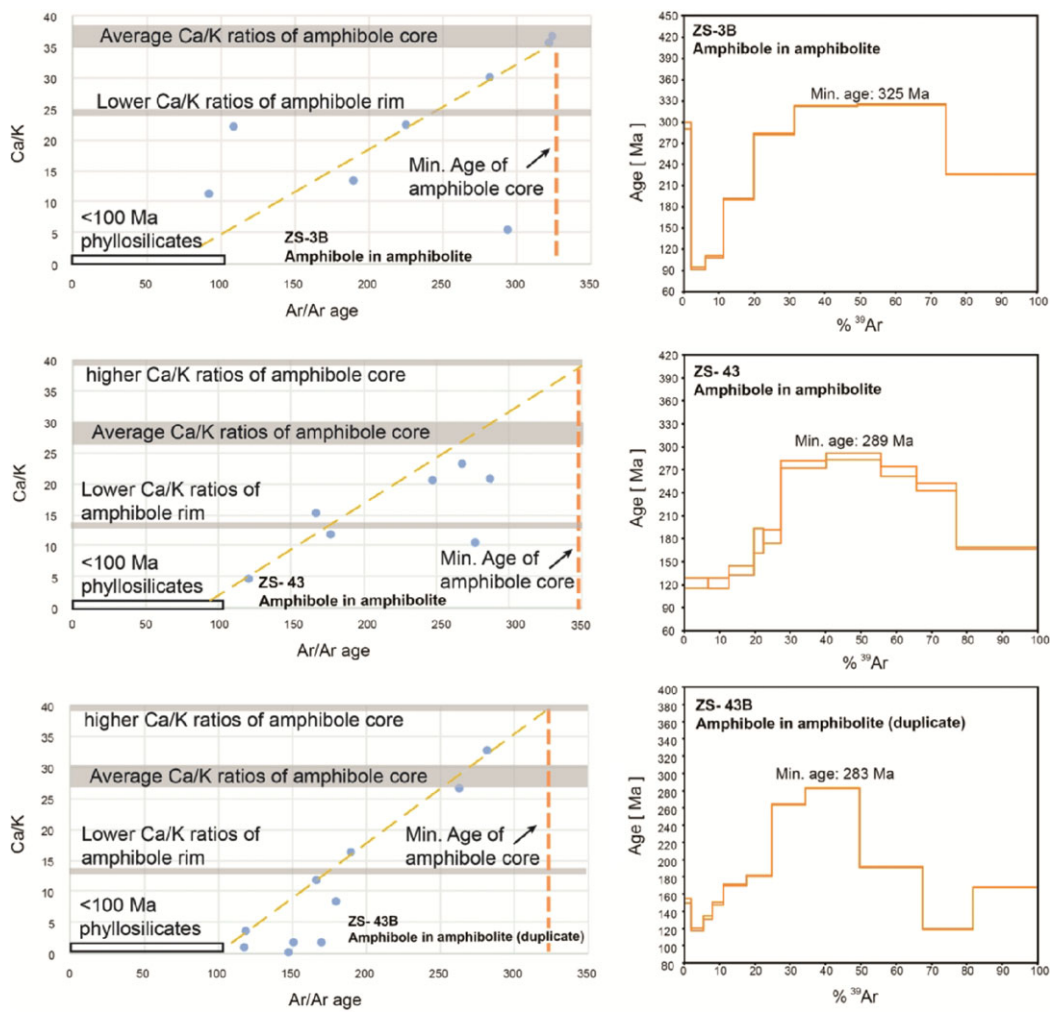


Fig. 9. (Colour online) ^{39}Ar - ^{40}Ar plateau ages (c. 174 to 248 Ma) for amphibole separates from the amphibolite samples.

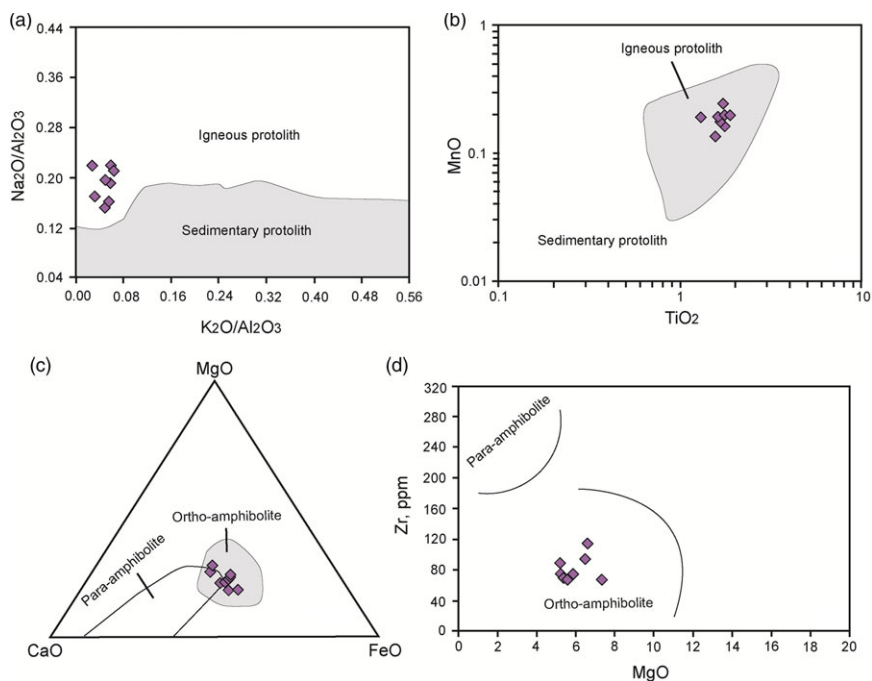


Fig. 10. (Colour online) Whole rock chemistry of the amphibolite samples indicates an igneous (ortho-amphibolite) protolith for them.

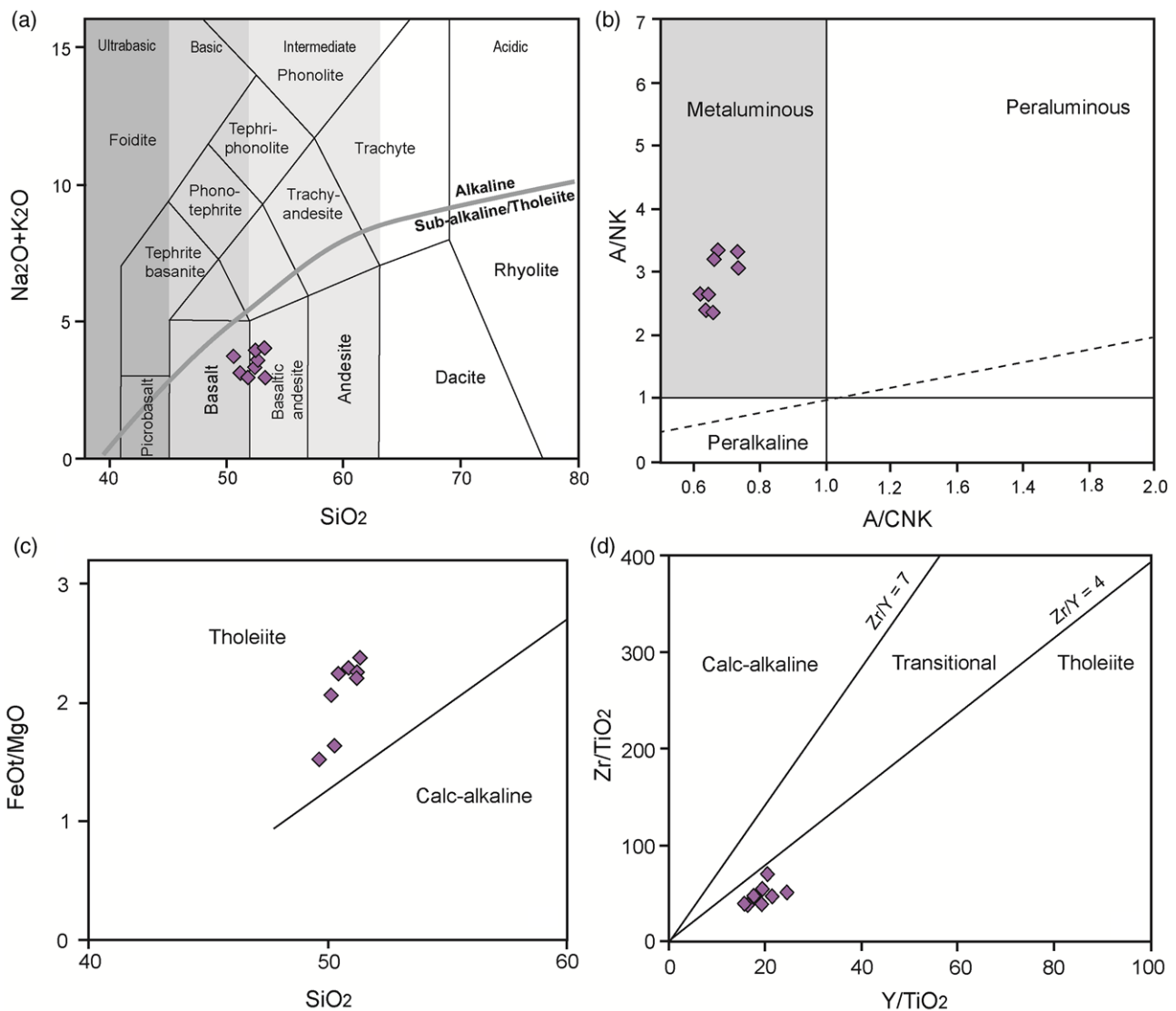


Fig. 11. (Colour online) The protolith of the amphibolite samples had a basalt to basaltic andesite lithology (a) and metaluminous (b) and tholeiitic (c, d) nature.

et al. 2005; Fig. 14b). The patterns in Figure 14 show enrichment in LILE (such as Rb, K, Pb, Sr and Ba), compared to HFSE. Some HFSE such as Ta, Nb, P and Ti show negative anomalies. LILE are mobile elements, released from the downgoing slab or associated sediments at relatively low temperatures, causing heterogeneity in the overlying mantle wedge (Stern *et al.* 1991; Pearce *et al.* 2005; Pearce & Stern, 2006), while all subduction-mobile elements including MREE, Pb, P, Th and Rb are released by super-critical fluids at higher temperature and depth (Woodhead, 1989; Elliott *et al.* 1997; Pearce & Stern, 2006). Considering enrichment of the samples in shallow subduction components, along with some enrichment in total subduction components, it seems that the magma-forming protolith of the amphibolites was enriched at shallow to medium depth of a subduction system. The samples show trace elements patterns similar to both island arc and back-arc basin basalts. Negative anomaly of Nb along with slight enrichment in LREE and LILE for the samples are features indicating arc-related magmatism for the protolith of the rocks. Ta–Nb–Th negative anomalies and Pb positive anomaly can indicate involvement of continental

crust or sedimentary material in the petrogenesis of the protolith (Saunders *et al.* 1992; Nagudi *et al.* 2003). All these features are in favour of a back-arc sialic setting for the formation of the studied mafic rocks.

Pelitic and semi-pelitic rocks studied here represent continental material, metamorphosed in the amphibolite facies; P – T estimates for both meta-sedimentary and meta-igneous rocks are consistent with a medium P –medium T regional gradient in response to collisional processes affecting continental crust or to a thick magmatic arc setting. The whole-rock chemistry of the amphibolites of the study area indicates a subduction-related affinity of the protolith and a possible back-arc sialic setting. In the continuation of the Allahyarlu–Hovai Fault, to the east of the Ahar Block, Rossetti *et al.* (2017) described HP rocks (blueschists to eclogites), which formed in the Early Carboniferous (*c.* 350 Ma, Ar–Ar dating). The formation of the Allahyarlu metamorphic complex is therefore found to be slightly younger but coherent with a metamorphic context bordering the Palaeotethys subduction zone. By analogy, to the west, in the Georgian Transcaucasus, a similar domain of high-temperature metamorphism is dated at 320–330 Ma

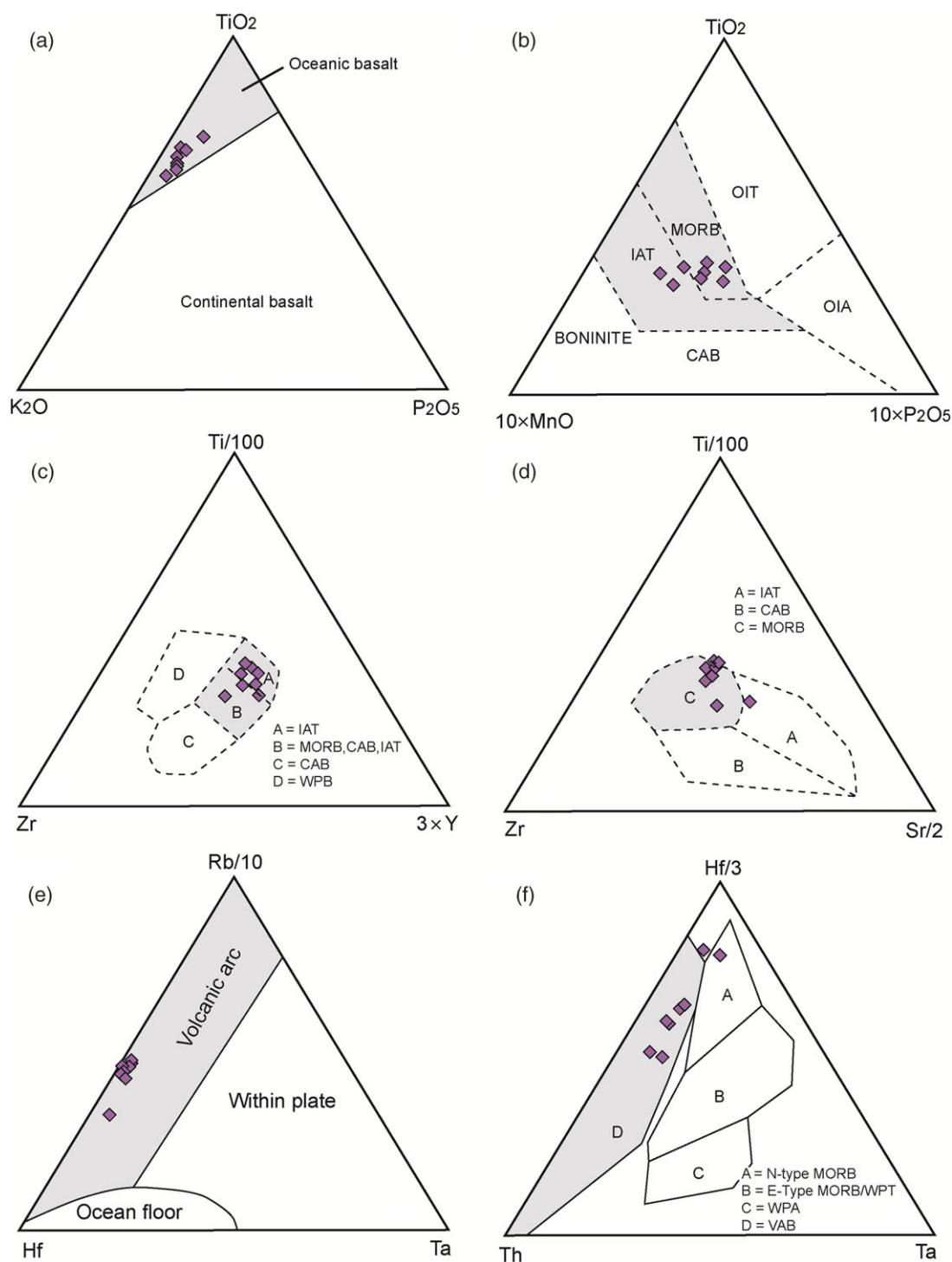


Fig. 12. (Colour online) The initial magma forming the protolith of the amphibolites was an oceanic basalt (a) and had island arc to MORB affinities (b, c, d). They were formed in a volcanic arc setting (e, f).

(Mayringer *et al.* 2011; Rolland *et al.* 2012), and is found directly south of a 350 Ma suture (Perchuk & Philippot, 1997). However, it is still difficult to correlate these occurrences as the Cenozoic deformation is quite complex and has offset the sutures due to strike-slip faults like the Araks or Talesh faults (Fig. 1). The geochemistry of igneous rocks from the study area (our unpublished data) is not indicative of a continental collision setting. These rocks show arc-related features and some adakitic signatures. Our findings are more compatible with a model

suggesting a long-lived active continental margin history for the southern margin of Eurasia, likely brought about by a northward subduction of Palaeotethys as in the Caucasus region (Rolland *et al.* 2011). In conclusion, the association of magmatic and metamorphic rocks of the Allahyarlu area is more in agreement with an active continental-margin magmatic arc during the Variscan orogeny and does not show any clear evidence of a continental collision. Figure 15 depicts a simple model for the tectonic setting of the Allahyarlu Variscan metamorphic rocks, where the MP–MT

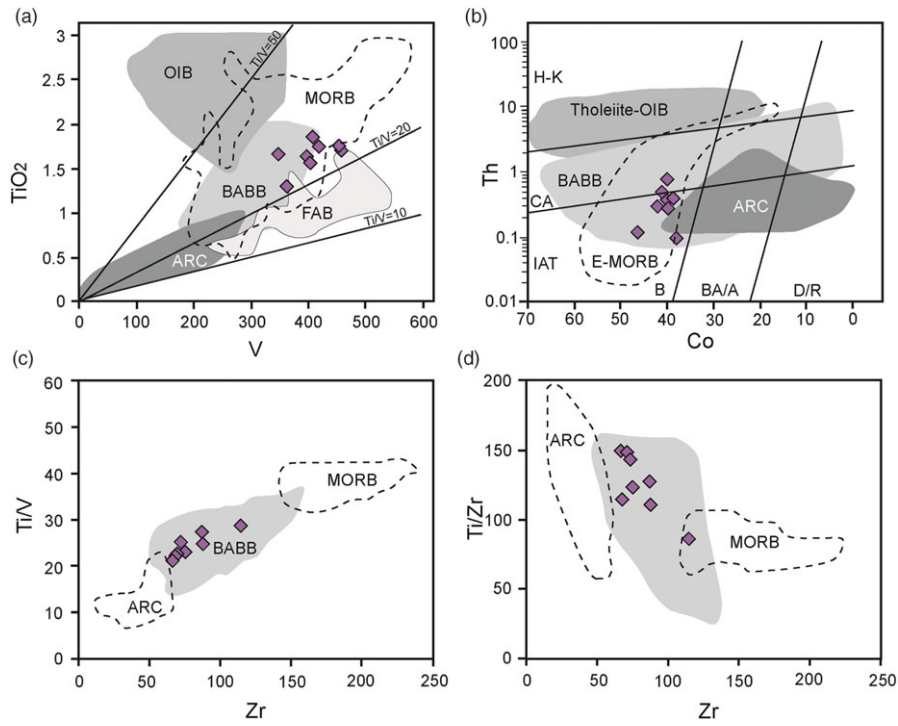


Fig. 13. (Colour online) A back-arc setting can be considered for the studied amphibolites based on immobile and trace elements contents.

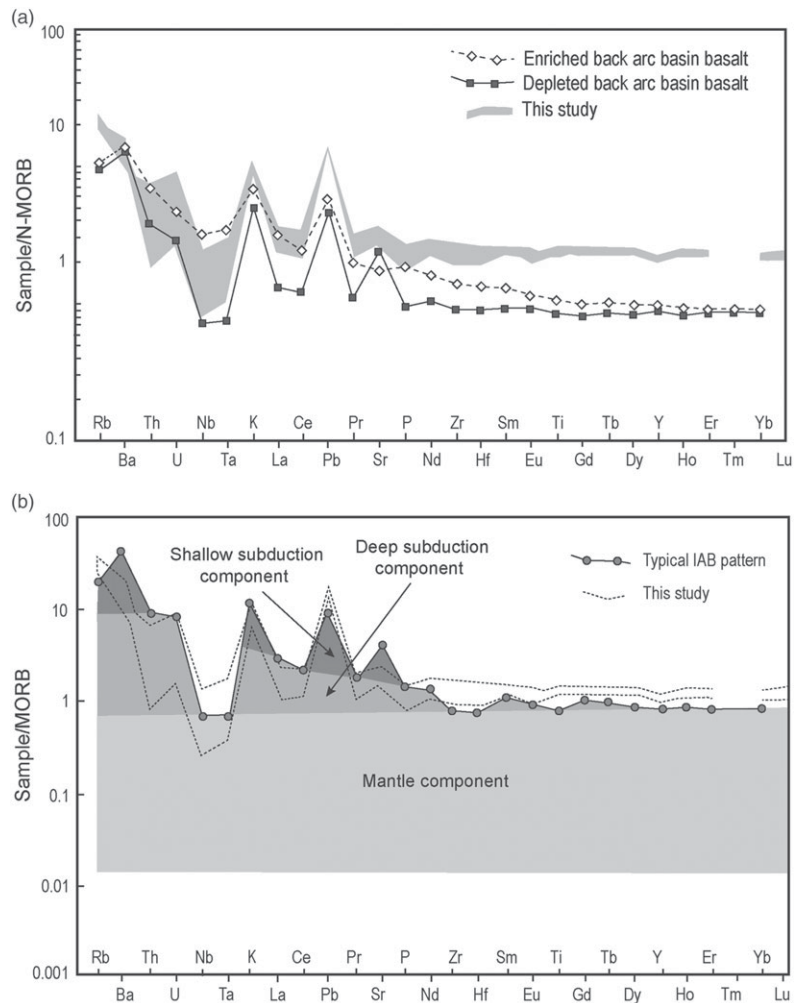


Fig. 14. Spider diagrams for the studied samples. The samples show similarities to both enriched and depleted back-arc basalts (a) and are more similar to typical island arc basalts, indicating shallow subduction components (b). The normalization values are from Sun & McDonough (1989).

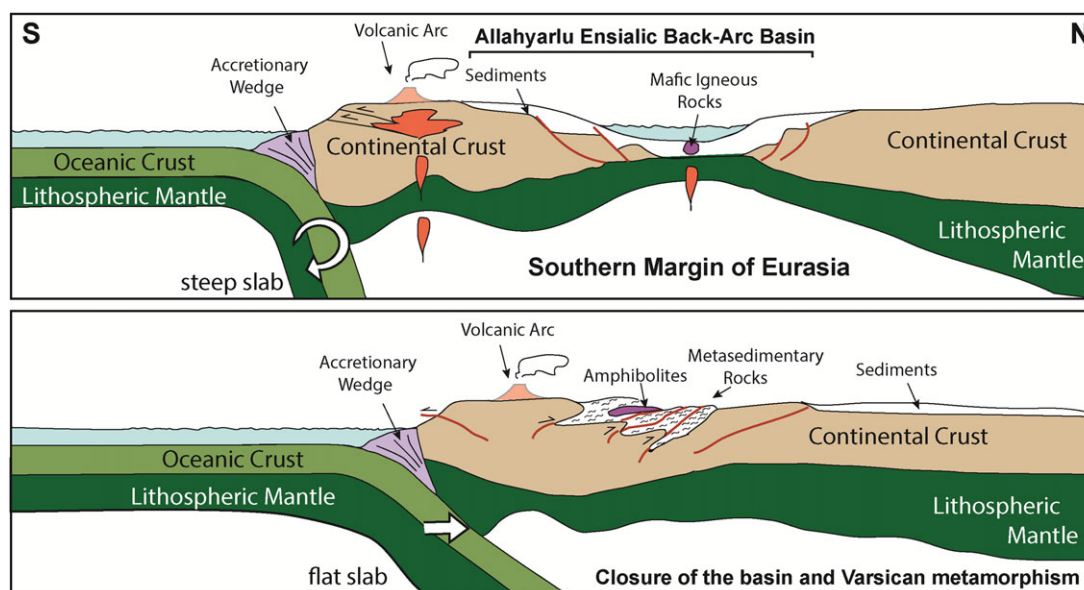


Fig. 15. (Colour online) A schematic model for the formation of the Variscan metamorphic rocks of the Allahyarlu area in NW Iran.

gradient could be related to a phase of active margin thickening due to flat-slab subduction (Fig. 15). In summary, the studied area is characterized by subduction of the Palaeotethys oceanic crust beneath the southern margin of Eurasia, which formed a thickened active continental margin including volcanic arc. The possible steep slab caused extension behind the volcanic arc and created an ensialic back-arc basin, in which protolith of meta-sedimentary rocks deposited. Also mafic rocks intruded within this extension zone, which made amphibolites later. The extensional basin transformed to a compressional one by changing of the steep slab into a flat slab. This caused metamorphism of the sedimentary and mafic igneous rocks in the amphibolite facies *c.* 326–334 Ma ago. The ophiolitic rocks, which are younger than the metamorphic rocks (*c.* 247 Ma; Z. Salimi, unpub. PhD thesis, Univ. Tabriz, 2019), were emplaced in the area. Further, the metamorphic rocks experienced a late greenschist facies deformation event, indicated by younger ages (<97 Ma) of amphibole. This may be related to a phase of tectonic reactivation due to an accretionary event which occurred in relation to the Neotethyan domain. The metamorphic and ophiolitic rocks were folded in a small anticline, then were covered by widespread and thick tertiary volcanic rocks.

Acknowledgements. This paper is a part of the PhD dissertation of Z.S., which is supported by University of Tabriz. We would like to thank Leila Rezaei and Mahleqa Rezaei Bargoshadi for their help with the field work. Thanks are also due to Jasper Berndt and Beate Schmitte for their help with the EMP analyses. Invaluable comments and suggestions by Federico Rossetti and an anonymous referee and great editorial contributions and help from Kathryn Goodenough are highly appreciated.

References

- Adamia SHA, Lordkipanidze MB and Zakariadze GZ (1977) Evolution of an active continental margin as exemplified by the Alpine history of the Caucasus. *Tectonophysics* **40**, 183–99.
- Aghanabati SA (2004) *Geology of Iran*. Tehran: Geological Survey of Iran, 708 pp. (in Persian).
- Babakhani AR and Nazer NH (1991) *Lahrud Geological Map*. Tehran: Geological Survey of Iran.
- Bagheri S and Stampfli GM (2008) The Anarak, Jandaq and Posht-e-Badam metamorphic complexes in central Iran: new geological data, relationships and tectonic implications. *Tectonophysics* **451**, 123–55.
- Barzegar A and Pourkermani M (2011) Structural evolution of folded zone of Allahyarlu in western Alborz. *Proceedings of the 21st Congress of Geological Sciences and 15th Congress of the Geological Survey of Iran, Urmia, Iran*. Tehran: Geological Survey of Iran.
- Berberian M and King GCP (1981) Towards a paleogeography and tectonic evolution of Iran. *Canadian Journal of Earth Sciences* **18**, 210–65.
- Berman RG (1988) Internally-consistent thermodynamic data for minerals in the system Na₂O-K₂O-CaO-MgO-FeO-Fe₂O₃-Al₂O₃-SiO₂-TiO₂-H₂O-CO₂. *Journal of Petrology* **29**, 445–522.
- Blundy JD and Holland TJB (1990) Calcic amphibole equilibria and a new amphibole-plagioclase geothermometer. *Contributions to Mineralogy and Petrology* **104**, 208–24.
- Blundy JD and Holland TJB (1994) Non-ideal interactions in calcic amphiboles and their bearing on amphibole-plagioclase thermometry. *Contributions to Mineralogy and Petrology* **116**, 433–47.
- Boulin J (1988) Hercynian and Eocimmerian events in Afghanistan and adjoining regions. *Tectonophysics* **148**, 253–78.
- Buchs DM, Bagheri S, Martin L, Herman J and Arculus R (2013) Palaeozoic to Triassic ocean opening and closure preserved in Central Iran: constraints from the geochemistry of meta-igneous rocks of the Anarak area. *Tectonophysics* **172–173**, 267–87.
- Büttner S and Kruhl JH (1997) The evolution of a late-Variscan high-T/low-P region: the southeastern margin of the Bohemian massif. *International Journal of Earth Sciences (Geologische Rundschau)* **86**, 21–38.
- Coish RA (1977) Ocean floor metamorphism in the Betts Cove ophiolite, Newfoundland. *Contributions to Mineralogy and Petrology* **60**, 255–70.
- De Capitani C and Brown TH (1987) The computation of chemical equilibrium in complex systems containing non-ideal solutions. *Geochimica et Cosmochimica Acta* **51**, 2639–52.
- Dercourt J, Ricou LE and Vrielynck B (eds) (1993) *Atlas Tethys, Palaeoenvironmental Maps*. Paris: Gauthier-Villars, 307 pp.
- Dickinson MP III and Hewitt DA (1986) A garnet-chlorite geothermometer. *Geological Society of America Abstracts with Programs* **18**, 584.
- Dokuz A (2011) A slab detachment and delamination model for the generation of Carboniferous high-potassium I-type magmatism in the Eastern Pontides, NE Turkey: the Köse composite pluton. *Gondwana Research* **19**, 926–44.
- Dokuz A, Uysal İ, Kaliwoda M, Karsli O, Ottley CJ and Kandemir R (2011) Early abyssal- and late SSZ-type vestiges of the Rheic oceanic mantle in the

- Variscan basement of the Sakarya Zone, NE Turkey: implications for the sense of subduction and opening of the Paleotethys. *Lithos* **127**, 176–91.
- Eftekharnejad J, Alavi-Naini M and Behrouzi A** (1993) *Geological Map of Torbate-Jam, Scale 1: 250,000 (one sheet)*. Tehran: Geological Survey of Iran.
- Elliott TR, Plank T, Zindler A, White W and Bourbon B** (1997) Element transport from slab to volcanic front at the Mariana Arc. *Journal of Geophysical Research* **102**, 14991–15019.
- Ernst WG and Liu J** (1998) Experimental phase-equilibrium study of Al- and Ti-contents of calcic amphibole in MORB – A semi-quantitative thermobarometer. *American Mineralogist* **83**, 952–69.
- Faryad SW and Kachlik V** (2013) New evidence of blueschist facies rocks and their geotectonic implication for Variscan suture(s) in the Bohemian Massif. *Journal of Metamorphic Geology* **31**, 63–82.
- Floyd PA and Winchester JA** (1978) Identification and discrimination of altered and metamorphosed volcanic rocks using immobile elements. *Chemical Geology* **21**, 291–306.
- Galoyan G, Rolland Y, Sosson M, Corsini M, Bilio S, Verati C and Melkonyan R** (2009) Geology, geochemistry and $^{40}\text{Ar}/^{39}\text{Ar}$ dating of Sevan ophiolites (Lesser Caucasus, Armenia): evidence for Jurassic back-arc opening and hot spot event between the South Armenian Block and Eurasia. *Journal of Asian Earth Sciences* **34**, 135–53.
- Gamkrelidze I, Shengelia D, Tsutsunava T, Chung S-L, Yichiu H and Chikhelidze KK** (2011) New data on the U-Pb zircon age of the Pre-alpine crystalline basement of the Black-Sea-Central Transcaucasian Terrane and their geological significance. *Bulletin of the Georgian National Academy of Sciences* **5**, 64–76.
- Garrels RM and Mackenzie FT** (1971) *Evolution of Sedimentary Rocks*. New York: Norton.
- Gerdes A, Wörner G and Henk A** (2000) Post-collisional granite generation and HT–LP metamorphism by radiogenic heating: the Variscan South Bohemian Batholith. *Journal of the Geological Society* **157**, 577–87.
- Ghent ED, Stout MZ, Black PM and Brothers RN** (1987) Chloritoid-bearing rocks associated with blueschists and eclogites, northern New Caledonia. *Journal of Metamorphic Geology* **5**, 239–54.
- Göncüoğlu MC, Turhan N, Şentürk K, Özcan A, Uysal Ş and Yaliniz MK** (2000) A geotraverse across northwestern Turkey: tectonic units of the central Sakarya region and their tectonic evolution. In *Tectonics and Magmatism in Turkey and the Surrounding Area* (eds Bozkurt E, Bozkurt JA, Piper JDA and Winchester JA), pp. 139–61. Geological Society of London, Special Publication no. 173.
- Graham CM and Powell R** (1984) A garnet–hornblende geothermometer: calibration, testing, and application to the Pelona Schist, Southern California. *Journal of Metamorphic Geology* **2**, 13–31.
- Grambling JA** (1990) Internally-consistent geothermometry and H_2O barometry in metamorphic rocks: the example garnet–chlorite–quartz. *Contributions to Mineralogy and Petrology* **105**, 617–28.
- Green TH and Hellman PL** (1982) Fe–Mg partitioning between coexisting garnet and phengite at high pressure, and comments on a garnet–phengite geothermometer. *Lithos* **15**, 253–66.
- Hässig M, Rolland R, Sahakyan L, Sosson M, Galoyan G, Avagyan A, Bosch D and Muller C** (2015) Multi-stage metamorphism in the South Armenian Block during the Late Jurassic to Early Cretaceous: tectonics over south-dipping subduction of Northern branch of Neotethys. *Journal of Asian Earth Sciences* **102**, 4–23.
- Holdaway MJ** (2000) Application of new experimental and garnet Margules data to the garnet–biotite geothermometer. *American Mineralogist* **85**, 881–92.
- Hynes A and Frost RC** (1988) Empirical garnet–muscovite geothermometry in low-grade metapelites, Selwyn Range (Canadian Rockies). *Journal of Metamorphic Geology* **6**, 297–309.
- Irvine TN and Baragar WRA** (1971) A guide to the chemical classification of the common volcanic rocks. *Canadian Journal of Earth Sciences* **8**, 523–48.
- Jamieson RA, Beaumont C, Fullsack P and Lee B** (1998) Barrovian regional metamorphism: where's the heat? In *What Drives Metamorphism and Metamorphic Reactions?* (eds Treloar PJ and O'Brien PJ), pp. 23–51. Geological Society of London, Special Publication no. 138.
- Kargaranbafghi F, Neubauer F and Genser J** (2015) Rapid Eocene extension in the Chapedony metamorphic core complex, Central Iran: constraints from $^{40}\text{Ar}/^{39}\text{Ar}$ dating. *Journal of Asian Earth Sciences* **106**, 156–68.
- Khalatbari Jafari M and Babaie HA** (2016) The geodynamics significance of the correlation of the Khoy ophiolites in northwest Iran with ophiolites in southeast Turkey. In *Tectonic Evolution, Collision and Seismicity of Southwest Asia: In Honor of Manuel Berberian's Forty-Five Years of Research Contributions* (ed. R. Sorkhabi), pp. 291–317. Geological Society of America Special Paper no. 525.
- Kohn MJ and Spear FS** (1989) Empirical calibration of geobarometers for the assemblage garnet + hornblende + plagioclase + quartz. *American Mineralogist* **74**, 77–84.
- Koppers AP** (2002) ArArCALC-software for $^{40}\text{Ar}/^{39}\text{Ar}$ age calculations. *Computers and Geosciences* **28**, 605–19.
- Krogh RE** (2000) The garnet–clinopyroxene Fe^{2+} –Mg geothermometer: an updated calibration. *Journal of Metamorphic Geology* **18**, 211–19.
- Krogh RE and Raheim A** (1978) Temperature and pressure dependence of Fe–Mg partitioning between garnet and phengite, with particular reference to eclogites. *Contributions to Mineralogy and Petrology* **66**, 75–80.
- Kröner U and Romer RL** (2013) Two plates – many subduction zones: the Variscan orogeny reconsidered. *Gondwana Research* **24**, 298–329.
- Mayringer F, Treloar PJ, Gerdes A, Finger F and Shengelia D** (2011) New age data from the Dzirula massif, Georgia: implications for the evolution of the Caucasian Variscides. *American Journal of Science* **311**, 404–41.
- Moghazi AM, Hassanen MA, Hashad MH and Mohamed FH** (2001) Garnet-bearing leucogranite in the El-Hudi area, southern Egypt: evidence of crustal anatexis during Pan-African low pressure regional metamorphism. *Journal of African Earth Sciences* **33**, 245–59.
- Nabavi MH** (1976) *An introduction to geology of Iran*. Tehran: Geological Survey of Iran Publications, 109 pp. (in Persian)
- Nagudi B, Koeberl C and Kura G** (2003) Petrography and geochemistry of the Singo granite, Uganda, and implications for its origin. *Journal of African Earth Sciences* **36**, 73–87.
- Nikishin AN, Ziegler PA, Bolotov SN and Fokin PA** (2011) Late Palaeozoic to Cenozoic evolution of the Black Sea–Southern Eastern Europe region: a view from the Russian platform. *Turkish Journal of Earth Sciences* **20**, 571–634.
- Okay AI and Şahinturk O** (1997) Geology of the Eastern Pontides. *American Association of Petroleum Geologists Bulletin* **68**, 291–311.
- Omrani H, Moazzen M, Oberhänsli R, Tsujimori T, Bousquet R and Moayyed M** (2013) Metamorphic history of glaucophane–paragonite–zoisite eclogites from the Shanderman area, northern Iran. *Journal of Metamorphic Geology* **31**, 791–812.
- Otten MT** (1984) The origin of brown hornblende in the Artfjället gabbro and dolerite. *Contributions to Mineralogy and Petrology* **86**, 189–99.
- Pearce JA and Cann JR** (1971) Ophiolite origin investigated by discriminant analysis using Ti, Zr and Y. *Earth and Planetary Science Letters* **12**, 339–49.
- Pearce JA and Cann JR** (1973) Tectonic setting of basic volcanic rocks determined using trace element analyses. *Earth and Planetary Science Letters* **19**, 290–300.
- Pearce JA and Stern RJ** (2006) Origin of back-arc basin magmas: trace element and isotope perspectives. In *Back-Arc Spreading Systems: Geological, Biological, Chemical, and Physical Interactions* (eds Christie DM, Fisher CR, Lee SM and Givens S), pp. 63–86. Washington, DC: American Geophysical Union, Geophysical Monograph Series, 166.
- Pearce JA, Stern RJ, Bloomer SH and Fryer P** (2005) Geochemical mapping of the Mariana arc–basin system: implications for the nature and distribution of subduction components. *Geochemistry, Geophysics, Geosystems* **6**, 1–17.
- Perchuk A and Philippot P** (1997) Rapid cooling and exhumation of eclogitic rocks from the Great Caucasus, Russia. *Journal of Metamorphic Geology* **15**, 299–310.
- Perchuk LL, Aranovich LY, Podlesskii KK, Lavrant'eva IV, Gerasimov VY, Fed'kin VV, Kitsul VI, Karsakov LP and Berdnikov NV** (1985) Precambrian granulites of the Aldan shield, eastern Siberia, USSR. *Journal of Metamorphic Geology* **3**, 265–310.
- Raase P** (1974) Al and Ti contents of hornblende, indicators of pressure and temperature of regional metamorphism. *Contributions to Mineralogy and Petrology* **45**, 231–6.
- Rolland Y** (2017) Caucasus collisional history: review of data from East Anatolia to West Iran. *Gondwana Research* **49**, 130–46.

- Rolland Y, Pernicek D, Kaymakci N, Sosson M, Barrier E and Avagyan A** (2012) Evidence for ~80–75 Ma subduction jump during Anatolide–Tauride–Armenian block accretion and ~48 Ma Arabia–Eurasia collision in Lesser Caucasus–East Anatolia. *Journal of Geodynamics* **56**, 76–85.
- Rolland Y, Sosson M, Adamia Sh and Sadradze N** (2011) Prolonged Variscan to Alpine history of an active Eurasian margin (Georgia, Armenia) revealed by ⁴⁰Ar/³⁹Ar dating. *Gondwana Research* **20**, 798–815.
- Rollinson HR** (1993) *Using Geochemical Data: Evaluation, Presentation, Interpretation*. New York: Longman Scientific and Technical, 352 pp.
- Romano SS, Brix MR, Dorr W, Fiala J, Krenn E and Zulauf G** (2006) The Carboniferous to Jurassic evolution of the pre-Alpine basement of Crete: constraints from U–Pb and U–(Th)–Pb dating of orthogneiss, fission-track dating of zircon, structural and petrological data. In *Tectonic Development of the East Mediterranean Region* (eds Robertson AHF and Mountrakis D), pp. 69–90. Geological Society of London, Special Publication no. 260.
- Rossetti F, Monié P, Nasrabi M, Theye T, Lucci F and Saadat M** (2017) Early Carboniferous subduction-zone metamorphism preserved within the Palaeo-Tethyan Rasht ophiolites (western Alborz, Iran). *Journal of the Geological Society* **174**, 741–58.
- Saunders AD, Storey M, Kent RW and Norry MJ** (1992) Consequences of plume–lithosphere interactions. In *Magmatism and the Causes for Continental Breakup* (eds Storey BC, Alabaster TS and Pankhurst RJ), pp. 41–60. Geological Society of London, Special Publication no. 68.
- Schmidt MW** (1992) Amphibole composition in tonalite as a function of pressure: an experimental calibration of the Al-in-hornblende barometer. *Contributions to Mineralogy and Petrology* **110**, 304–10.
- Şengör AMC and Yilmaz Y** (1981) Tethyan evolution of Turkey: a plate tectonic approach. *Tectonophysics* **75**, 181–90.
- Şengör AMC, Yilmaz Y and Sungurlu O** (1984) Tectonics of the Mediterranean Cimmerides: nature and evolution of the western termination of Palaeo-Tethys. In *The Geological Evolution of the Eastern Mediterranean* (eds Dixon JE and Robertson AHF), pp. 77–112. Geological Society of London, Special Publication no. 17.
- Shafaii Moghadam H, Corfu F, Stern RJ and Lotfibakhsh A** (2018) The Eastern Khoys metamorphic complex of NW Iran: a Jurassic ophiolite or continuation of the Sanandaj–Sirjan Zone? *Journal of the Geological Society* **176**, 517–29. doi: [10.1144/jgs2018-081](https://doi.org/10.1144/jgs2018-081).
- Shafaii Moghadam H, Ghorbani G, Khedr MZ, Fazlnia N, Chiardia M, Eyuboglu Y, Santosh M, Francisco CG, Martinez ML, Gourgaud A and Arai S** (2014) Late Miocene K-rich volcanism in the Eslamieh Peninsula (Saray), NW Iran: implications for geodynamic evolution of the Turkish–Iranian High Plateau. *Gondwana Research* **26**, 1028–50.
- Shafaii Moghadam H, Li XH, Ling XX, Stern RJ, Khedr MZ, Chiardia M, Ghorbani G, Arai S and Tamura A** (2015) Devonian to Permian evolution of the Paleo-Tethys Ocean: new evidence from U–Pb zircon dating and Sr–Nd–Pb isotopes of the Darrehanjir–Mashhad “ophiolites”, NE Iran. *Gondwana Research* **28**, 781–99.
- Shervais JW** (1982) Ti–V plots and the petrogenesis of modern and ophiolitic lavas. *Earth and Planetary Science Letters* **59**, 101–18.
- Somin ML** (1991) Geological characteristics of the metamorphic complexes of the Great Caucasus. In *The Petrology of Metamorphic Complexes of the Great Caucasus* (ed. Korikovskiy SP), pp. 8–43. Moscow: Nauka.
- Stampfli GM** (1978) *Etude géologique générale de l'Elbourz oriental au sud de Gonbad-e-Qabus (Iran NE)*. PhD thesis, Université de Genève, Geneva, Switzerland. Published thesis.
- Stampfli GM and Borel GD** (2002) A plate tectonic model for the Paleozoic and Mesozoic constrained by dynamic plate boundaries and restored synthetic oceanic isochrones. *Earth and Planetary Science Letters* **196**, 17–33.
- Steiger RH and Jäger E** (1977) Subcommittee on geochronology: convention on the use of decay constants in geo- and cosmochronology. *Earth and Planetary Science Letters* **36**, 359–62.
- Stein E and Dietl C** (2001) Hornblende thermobarometry of granitoids from the Central Odenwald (Germany) and their implications for the geotectonic development of the Odenwald. *Mineralogy and Petrology* **72**, 185–207.
- Stern RJ, Morris J, Bloomer SH and Hawkins JW** (1991) The source of the subduction component in convergent margin magmas: trace element and radiogenic isotope evidence from Eocene boninites, Mariana forearc. *Geochimica et Cosmochimica Acta* **55**, 1467–81.
- Stöcklin J** (1968) Structural history and tectonics of Iran: a review. *American Association of Petroleum Geologists Bulletin* **52**, 1229–58.
- Stöcklin J** (1977) Structural correlation of the Alpine ranges between Iran and Central Asia. *Mémoires de la Société Géologique de France* **8**, 333–53.
- Sudi Ajirlu M and Moazzen M** (2014) The role of the Allahyarlu ophiolite in the tectonic evolution of NW Iran and adjacent areas (Late Carboniferous–Recent). *Central European Geology* **57**, 363–83.
- Sun SS and McDonough WF** (1989) Chemical and isotopic systematics of oceanic basalts: implications for mantle composition and processes. In *Magmatism in the Ocean Basins* (eds Saunders AD and Norry MJ), pp. 313–45. Geological Society of London, Special Publication no. 42.
- Topuz G, Altherr R, Kalt A, Satir M, Werner O and Schwarz WH** (2004b) Aluminous granulites from the Pular complex, NE Turkey: a case of partial melting, efficient melt extraction and crystallization. *Lithos* **72**, 183–207.
- Topuz G, Altherr R, Satir M and Schwarz WH** (2004a) Low-grade metamorphic rocks from the Pular complex, NE Turkey: implications for the pre-Liassic evolution of the Eastern Pontides. *International Journal of Earth Sciences* **93**, 72–91.
- Topuz G, Altherr R, Schwarz WH, Dokuz A and Meyer H-P** (2007) Variscan amphibolite-facies rocks from the Kurtoğlu metamorphic complex (Gümüşhane area, Eastern Pontides, Turkey). *International Journal of Earth Sciences* **96**, 861–73.
- Topuz G, Göçmengil G, Rolland Y, Celik ÖF, Zack T and Schmitt AK** (2013) Jurassic accretionary complex and ophiolite from northeast Turkey: no evidence for the Cimmerian continental ribbon. *Geology* **41**, 255–58.
- Turner DL, Forbes RB and Dillon JT** (1971) K–Ar geochronology of the south western Brooks Range, Alaska. *Canadian Journal of Earth Sciences* **16**, 1789–804.
- Ustaömer T and Robertson AHF** (1993) A Late Palaeozoic–Early Mesozoic marginal basin along the active southern continental margin of Eurasia: evidence from the central Pontides (Turkey) and adjacent regions. *Geological Journal* **28**, 219–38.
- Ustaömer T, Robertson AHF, Ustaömer PA, Gerdes A and Peytcheva I** (2013) Constraints on Variscan and Cimmerian magmatism and metamorphism in the Pontides (Yusufeli–Artvin area), NE Turkey from U–Pb dating and granite geochemistry. In *Geological Development of Anatolia and the Easternmost Mediterranean Region* (eds Robertson AHF and Ünlügenç UC), pp. 49–74. Geological Society of London, Special Publication no. 372.
- Walker KR, Joplin GA, Lovering JF and Green R** (1959) Metamorphic and metasomatic convergence of basic igneous rocks and lime-magnesia sediments of the Precambrian of North-western Queensland. *Journal of the Geological Society of Australia* **6**, 149–77.
- Werner CD** (1987) Saxonian granulites–igneous or lithogenous. A contribution to the geochemical diagnosis of the original rocks in high-metamorphic complexes. In: Grestenberger, H. ed., *Contribution to the geology of the Saxonian granulite massif*. *ZfL-Mitteilungen* **133**, 221–250.
- Whitney D and Evans BW** (2010) Abbreviations for names of rock-forming minerals. *The American Mineralogist* **95**, 185–87.
- Woodhead JD** (1989) Geochemistry of the Mariana arc (western Pacific): source composition and processes. *Chemical Geology* **76**, 1–24.
- Wu CM, Wang XS and Yang CH** (2002) Empirical garnet–muscovite geothermometry in metapelites. *Lithos* **62**, 1–13.
- Wu C-M and Zhao G** (2006) Recalibration of the garnet–muscovite (GM) geothermometer and the garnet–muscovite–plagioclase–quartz (GMPQ) geobarometer for metapelitic assemblages. *Journal of Petrology* **47**, 2357–68.
- Zakariadze GS, Karpenko SF and Bazilev BA** (1998) Petrology, geochemistry and Sm–Nd isotopic age of Pre-Late-Hercynian paleo-oceanic complex of Dzirula salient of Transcaucasian massif. *Journal of Petrology* **6**, 422–44.
- Zanchi A, Malaspina N, Zanchetta S, Berra F, Benciolini L, Bergomi M, Cavallo A, Javadi HR and Kouhpeyma M** (2015) The Cimmerian accretionary wedge of Anarak, Central Iran. *Journal of Asian Earth Sciences* **102**, 45–72.
- Zulauf G, Romano SS, Dorr W and Flala J** (2007) Crete and the Minoan terranes: age constraints from U–Pb dating of detrital zircons. *Geological Society of America Special Paper* **423**, 401–11.

Appendix: Summary of obtained Ar–Ar data

Incremental heating steps	Heating % ³⁹ Ar	³⁶ Ar(a) [fA]	³⁷ Ar(ca) [fA]	³⁸ Ar(cl) [fA]	³⁹ Ar(k) [fA]	⁴⁰ Ar(r) [fA]	Age ± 1 s (Ma)	⁴⁰ Ar(r) (%)	³⁹ Ar(k) (%)	K/Ca	± 1 s
Sample ZS-1-12 muscovite; $J = 0.00677800 \pm 0.00000474$; plateau age 333.7 ± 0.8 Ma; total fusion age 333.7 ± 0.3 Ma; isochron age 338.2 ± 2.0 Ma; inverse isochron age 334.5 ± 1.3 Ma.											
ZS01-12_04102018_01	6.0 %	0.1010549	0.0000000	0.460818	2.92474	62.0578	242.99 ± 3.84	67.22	0.97	–	
ZS01-12_04102018_02	8.0 %	0.0353482	1.1228033	0.022410	6.47328	190.2448	328.49 ± 2.26	94.65	2.15	2.5	± 12.8
ZS01-12_04102018_03	10.0 %	0.0419229	0.0000000	0.000000	22.67034	684.3963	336.65 ± 0.65	98.11	7.53	–	
ZS01-12_04102018_04	12.0 %	0.0757742	0.0000000	0.000000	57.92045	1718.7971	331.41 ± 0.31	98.60	19.23	–	
ZS01-12_04102018_05	14.0 %	0.0447679	0.4764159	0.000000	57.28832	1707.6493	332.76 ± 0.30	99.13	19.02	51.7	± 528.7
ZS01-12_04102018_06	16.0 %	0.0255805	0.0000000	0.000000	52.60948	1583.1225	335.66 ± 0.29	99.42	17.47	–	
ZS01-12_04102018_07	18.0 %	0.0254475	2.8381110	0.000000	22.31175	661.6611	331.21 ± 0.62	98.77	7.41	3.4	± 4.6
ZS01-12_04102018_08	20.0 %	0.0581523	0.0000000	0.000000	15.10391	450.6909	333.08 ± 0.78	96.20	5.02	–	
ZS01-12_04102018_09	24.0 %	0.0098259	0.0000000	0.002539	21.08810	633.6154	335.19 ± 0.53	99.44	7.00	–	
ZS01-12_04102018_10	30.0 %	0.0070619	0.2392954	0.000000	25.81969	782.4542	337.82 ± 0.98	99.63	8.57	46.4	± 881.7
ZS01-12_04102018_11	35.0 %	0.0000000	0.0000000	0.000000	5.84136	177.3161	338.34 ± 3.74	99.90	1.94	–	
ZS01-12_04102018_12	100.0 %	0.0194666	0.0000000	0.098566	11.09217	352.5116	352.76 ± 2.19	98.29	3.68	–	
Sample ZS-1-15 muscovite; $J = 0.00677900 \pm 0.00000475$; plateau age 325.7 ± 0.8 Ma; total fusion age 323.6 ± 0.2 Ma; isochron age 324.0 ± 1.3 Ma; inverse isochron age 323.0 ± 1.9 Ma.											
ZS-15_05102018_01	6.0 %	0.0589046	–	1.1194306	3.29148	48.418	171.89 ± 2.68	73.25	0.94	–	
ZS-15_05102018_02	8.0 %	0.0422102	0.724596	0.1690634	8.65669	239.774	311.16 ± 1.51	94.91	2.47	5.14	± 28.17
ZS-15_05102018_03	10.0 %	0.0141044	–	0.0508347	18.16584	530.114	326.41 ± 0.72	99.11	5.18	–	
ZS-15_05102018_04	12.0 %	0.0254197	1.253961	0.1375142	39.81195	1169.793	328.47 ± 0.29	99.26	11.34	13.65	± 53.68
ZS-15_05102018_05	14.0 %	0.0147076	7.396474	0.0705258	38.67239	1121.350	324.51 ± 0.40	99.51	11.02	2.25	± 1.57
ZS-15_05102018_06	16.0 %	0.0098521	–	0.0180889	50.86792	1488.941	327.32 ± 0.26	99.70	14.49	–	
ZS-15_05102018_07	18.0 %	0.0136006	2.186952	0.0000000	49.13965	1420.603	323.62 ± 0.27	99.61	14.00	9.66	± 15.57
ZS-15_05102018_08	20.0 %	0.0048724	5.098890	0.0000000	24.39623	693.852	318.81 ± 0.63	99.69	6.95	2.06	± 0.99
ZS-15_05102018_09	24.0 %	0.0036088	4.614198	0.0000000	26.28640	764.308	325.33 ± 0.56	99.76	7.49	2.45	± 2.81
ZS-15_05102018_10	100.0 %	0.0700121	6.500578	0.2683327	91.68455	2666.859	325.45 ± 0.18	99.12	26.12	6.06	± 3.46
Sample ZS-3B amphibole; $J = 0.00678000 \pm 0.00000475$; plateau age –; total fusion age 263.0 ± 0.4 Ma.											
ZS3B_10102018_01	6.0 %	0.1465599	4.4988	1.1869169	1.948680	50.9412	295.07 ± 4.41	53.76	2.17	0.1863	± 0.2016
ZS3B_10102018_02	9.0 %	0.0345891	17.2885	0.2816816	3.621695	28.3136	93.40 ± 1.47	73.07	4.04	0.0901	± 0.0237
ZS3B_10102018_03	13.0 %	0.0813460	43.0990	0.3701921	4.602807	42.3915	109.53 ± 1.34	63.45	5.13	0.0459	± 0.0048
ZS3B_10102018_04	17.0 %	0.0965506	43.8353	0.3963420	7.673054	126.1932	191.17 ± 0.91	81.29	8.55	0.0753	± 0.0074
ZS3B_10102018_05	21.0 %	0.0805757	131.6762	0.7732095	10.281048	256.9093	283.02 ± 0.77	91.34	11.46	0.0336	± 0.0011
ZS3B_10102018_06	25.0 %	0.1648518	243.5698	1.5563987	16.033363	461.9368	322.66 ± 0.64	90.29	17.88	0.0283	± 0.0005
ZS3B_10102018_07	30.0 %	0.1676646	349.9088	2.3209538	22.376935	649.6477	324.92 ± 0.75	92.76	24.95	0.0275	± 0.0003
ZS3B_10102018_08	35.0 %	0.1332388	220.6965	1.3812625	23.157049	455.0318	226.16 ± 0.45	91.83	25.82	0.0451	± 0.0006
Sample ZS-X43 amphibole; $J = 0.00677800 \pm 0.00000474$; plateau age –; total fusion age 214 ± 1 Ma.											
ZS-X43_04102018_01	6.0 %	0.0466586	2.318114	0.1311691	1.219808	12.59709	122.34 ± 6.41	47.42	6.75	0.226	± 0.393
ZS-X43_04102018_02	8.0 %	0.0141593	–	0.0309941	1.044736	10.80271	122.49 ± 6.88	71.73	5.78	–	